Projet de hadronthérapie à Lyon
Revue de l'injection dans PIMMS
et variantes : protons de 7 MeV, injection extérieure

F. Méot*, A. Tkatchenko†

June 6, 2001

Abstract

Ce rapport passe en revue certaines études concernant l'injection dans le synchrotron, réalisées sur la base du document PIMMS du Cern, dans le cadre et en tenant compte des spécificités du projet de hadronthérapie Rhône-Alpes. Deux variantes sont aussi présentées, injection de protons de 7 MeV et injection par l'extérieur de l'anneau.

CEA DSM DAPNIA/SEA-01-09 & CNRS IN2P3 IPNO-01-06

*CEA, DSM/DAPNIA/SEA, 91191 Saclay (fmeot@cea.fr)
†CNRS IN2P3/IPN, 91400 Orsay (tkatchen@ipno.in2p3.fr)

Contents

1 Introduction

In the frame of the project of hadrontherapy installation at Lyon [1], various parameters of the PIMMS [2] design that project is based on are reviewed. In particular, 7 MeV proton injection is assessed, as well as injection from outwards.

Two Saclay codes are used for these studies [3, 4], with the goal, amongst others, to provide comparisons with PIMMS methods based on Winagile [5] code. Various things are also done using mAD [6].

2 Basic ring features, working hypothesis

We first state basic properties of the first order optics, as drawn from PIMMS, to be referred to in the sequel.

2.1 Lattice, injection optics

Carbon

Figure 1 shows the optical functions for the Carbon C^{6+} injection as obtained with quadrupole strengths $KF1 = 0.319185, KF2 = 0.526045, KD = -0.527744$, together with beam envelopes $\sqrt{\beta(s)\epsilon_{x,z}/\pi + (D_x(s)\delta p/p)^2}$ for the nominal stored emittance values $\epsilon_x/\pi = \epsilon_z/\pi =$ 30 10^{-6} m.rad and momentum spread $\delta p/p = \pm 1.2\ 10^{-3}$ centered on $< \delta p/p >= 0$, next to multiturn injection. Note that, the injected Carbon beam is to be centered on $< \delta p/p >= -0.0021$ (Section 3.1) so that it will in fact be shifted by $-0.0021 D_x(s)$ (towards negative x regions) in the non-zero dispersion sections.

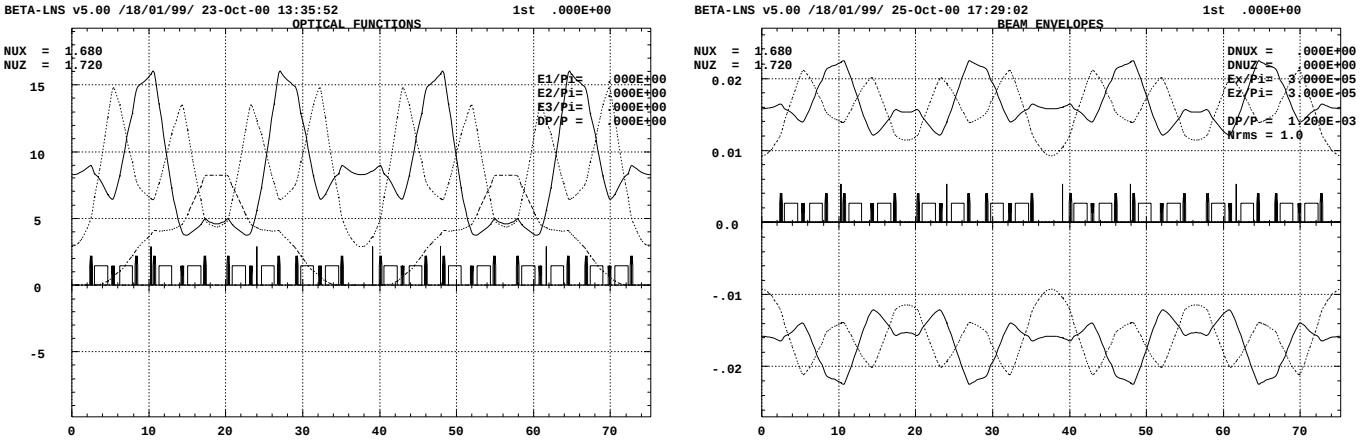

Figure 1: Carbon case, injection. Left : optical functions. Right : envelopes of stored beam for $\epsilon_x/\pi = \epsilon_z/\pi = 30\ 10^{-6}$ m.rad, $\delta p/p = \pm 1.2\ 10^{-3}$, $< \delta p/p >= 0$.

Ensuing tunes are $\nu_x = 1.68, \nu_z = 1.72$. The horizontal closed orbit bump excited at injection (Section 3.1) induces vertical tune change up to +0.01 due to residual closed orbit in sextupoles beyond the bump.

Natural chromaticities are $\delta\nu_x/\delta p/p = -0.61, \delta\nu_z/\delta p/p = -1.76$. Induced chromaticities with integrated sextupole strengths $S_D L = -0.2378, S_F L = 0.2127$ are[1] $\delta\nu_x/\delta p/p =$

[1] Winagile delivers slightly different values, natural chromaticities $\delta\nu_x/\delta p/p = -0.66, \delta\nu_z/\delta p/p = -0.962$, induced chromaticities $\delta\nu_x/\delta p/p = -3.63, \delta\nu_z/\delta p/p = -2.672$.

$-3.58, \delta\nu_z/\delta p/p = -3.47$. Given the chromaticity sextupole strengths above, tune shifts with amplitude are $\delta\nu_x/\epsilon_x/\pi = 37.4, \delta\nu_x/\epsilon_z/\pi = -27.1, \delta\nu_z/\epsilon_z/\pi = 20.7$.

Off momentum beam : As stressed above the Carbon beam is stored $< \delta p/p >= -0.0021$ off-momentum, ensuing tunes and chromaticities become, with quad and sextupoles settings as above,
$\nu_x = 1.690161, \nu_z = 1.72$, $\delta\nu_x/\delta p/p = -4.158, \delta\nu_z/\delta p/p = -3.160$ (MAD data).

Proton, 20 MeV and 7 MeV

The Fig. 2 shows the optical functions for proton injection as obtained with quadrupole strengths $KF1 = 0.360104, KF2 = 0.545078, KD = -0.587004$, at both energies of 20 MeV and 7 MeV. Indeed, 7 MeV injection is foreseen with half the 20 MeV stored beam intensity [7], so that the overall space-charge tune shift is but slightly smaller at 7 MeV, which we choose to neglect for simplicity (Fig. 3) :

let $\Delta\nu \approx \frac{N}{S\beta^2\gamma^3} \approx \frac{N}{S(\beta\gamma)^2}$ be the space-charge tune shift, $S_{D,F}$ the sextupole strengths, N the number of particles in the stored beam, $\beta\gamma = (c^2/v^2 - 1)^{-1/2}$ with v =particle velocity,

by changing $S_{D,F} \to 1.696 S_{D,F}$, $\beta\gamma \to \beta\gamma/1.696$, $N \to N/2 = 1.15\ 10^{11}$ stored particles at 7 MeV,

one gets the tune shifts $\Delta\nu|_{7\ MeV} = \frac{N/2}{1.696 S \times (\beta/1.696)^2} \approx 0.85 \Delta\nu|_{20\ MeV} = 1.675$ (horizontal) and 1.718 (vertical) at 7 MeV.

Beam envelopes $\sqrt{\beta(s)\epsilon_{x,z}/\pi + (D_x(s)\delta p/p)^2}$ in Fig. 3 are obtained,
- in the 20 MeV case with the nominal stored emittance values $\epsilon_x/\pi = \epsilon_z/\pi = 12.5\ 10^{-6}$ m.rad and momentum spread $\delta p/p = \pm 1.2\ 10^{-3}$ centered on $< \delta p/p >= 0$ next to multiturn injection (note that, the 20 MeV injected beam is to be centered on $< \delta p/p >= -0.0018$ entailing in fact an additional x-shift of $-0.0018 D_x(s)$ in the non-zero dispersion regions) ;
- in the 7 MeV case with the stored emittance values $\epsilon_x/\pi = \epsilon_z/\pi = 21\ 10^{-6}$ m.rad (i.e., $\beta\gamma|_{20\ MeV}/\beta\gamma|_{7\ MeV} = 1.696$ times the 20 MeV emittances) and momentum spread $\delta p/p = \pm 2\ 10^{-3}$ (1.696 times the 20 MeV case) centered on $< \delta p/p >= 0$ (the 7 MeV injected beam will be centered on $< \delta p/p >= -0.0018$).

Working tunes from quadrupole strengths above used as multiturn injection conditions (the upper values in both tune diagrams of Fig. 3) are $\nu_x = 1.764210, \nu_z = 1.829251$. The horizontal closed orbit bump excited at injection (Section 3.1) induces vertical tune decrease up to -0.015 due to non-zero residual closed orbit in sextupoles beyond the bump.

Natural chromaticities are $\delta\nu_x/\delta p/p = -0.69, \delta\nu_z/\delta p/p = -2$. Induced chromaticities with integrated sextupole strengths $S_D L = -0.178537, S_F L = 0.0481237$ are[2] $\delta\nu_x/\delta p/p = -3.93, \delta\nu_z/\delta p/p = -1.34$. Given the chromaticity sextupole strengths above, tune shifts with amplitude are $\delta\nu_x/\epsilon_x/\pi = 29, \delta\nu_x/\epsilon_z/\pi = -9.8, \delta\nu_z/\epsilon_z/\pi = 5.8$.

Off momentum beam : The proton beam is stored $< \delta p/p >= -0.0018$ off-momentum, ensuing tunes and chromaticities become, with quad and sextupoles settings as above,
$\nu_x = 1.773367, \nu_z = 1.829334$, $\delta\nu_x/\delta p/p = -4.3112, \delta\nu_z/\delta p/p = -1.2362$ (MAD data).

[2]Winagile delivers slightly different vertical chromaticity $\delta\nu_z/\delta p/p = -0.60$.

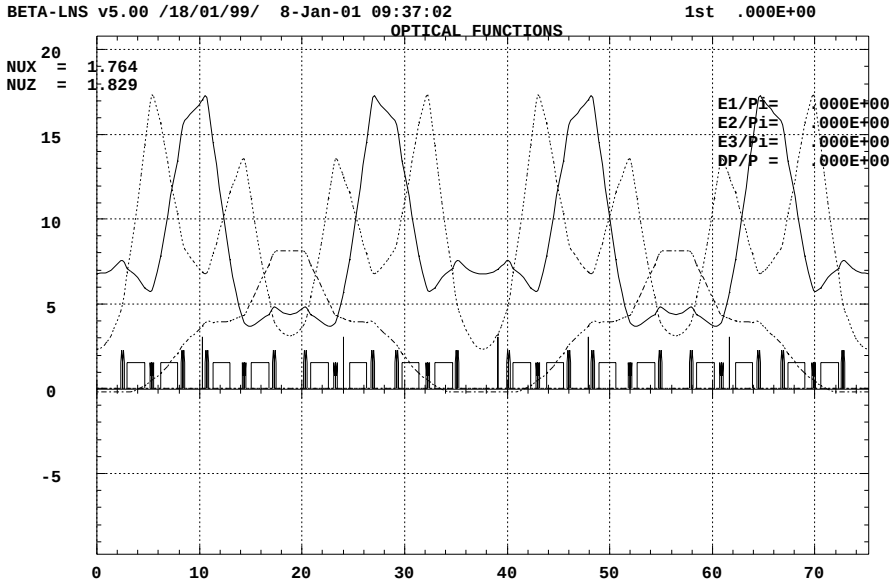

Figure 2: Proton injection, optical functions, 20 MeV and 7 MeV.

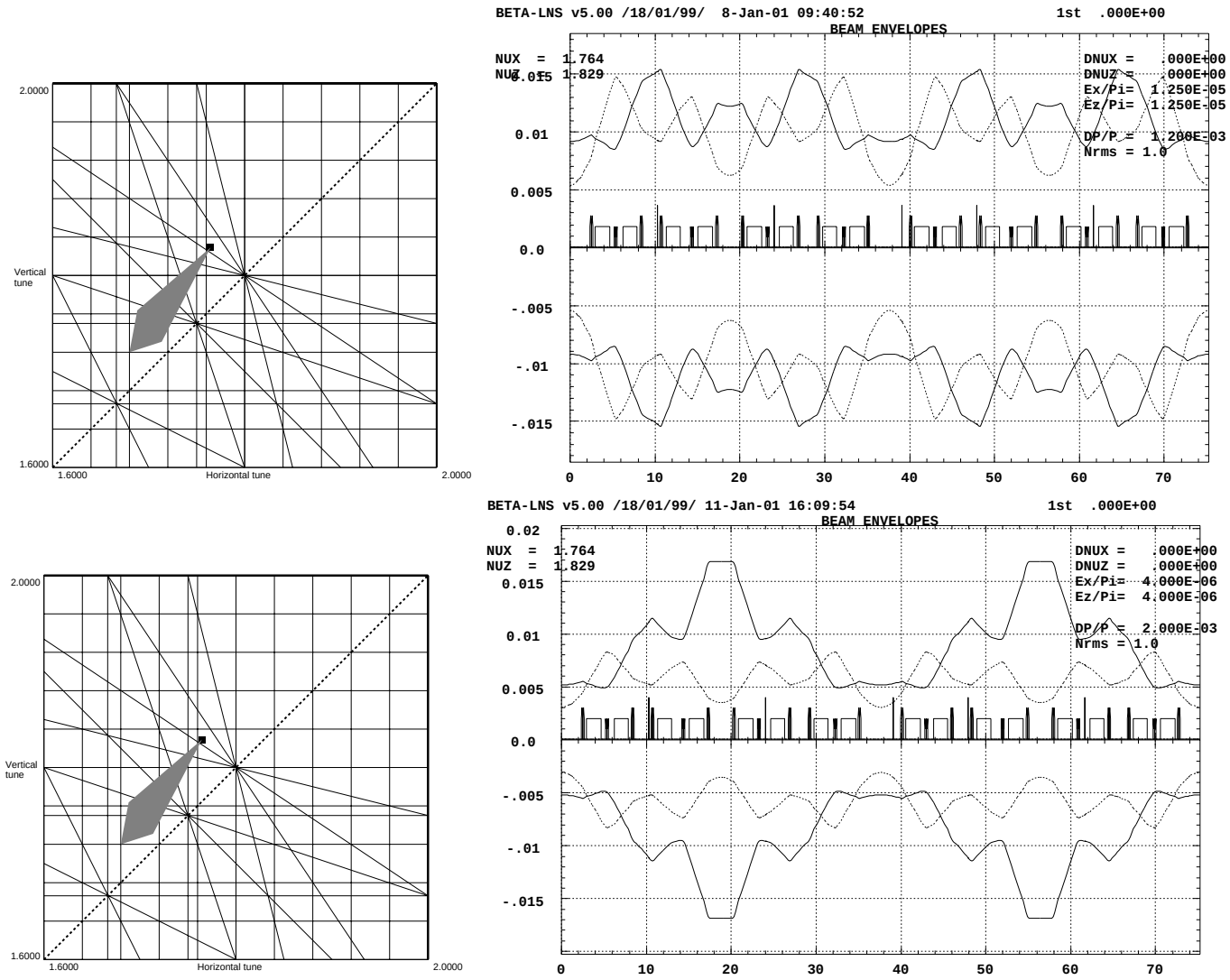

Figure 3: Proton injection, tune diagrams (from Winagile) and stored beam envelopes. Top row : 20 MeV ; $\epsilon_x/\pi = \epsilon_z/\pi = 12.5\ 10^{-6}$ m.rad, $\delta p/p = \pm 1.2\ 10^{-3}$. Bottom row : 7 MeV ; $\epsilon_x/\pi = \epsilon_z/\pi = 21\ 10^{-6}$ m.rad, $\delta p/p = \pm 2\ 10^{-3}$.

2.2 Geometrical aperture

The geometrical acceptance gives an estimate of the clearance with respect to the injected beam. It is obtained in the following after transverse apertures accounted for in Winagile data files as displayed in Fig.4, that however shows that the acceptance is mostly determined

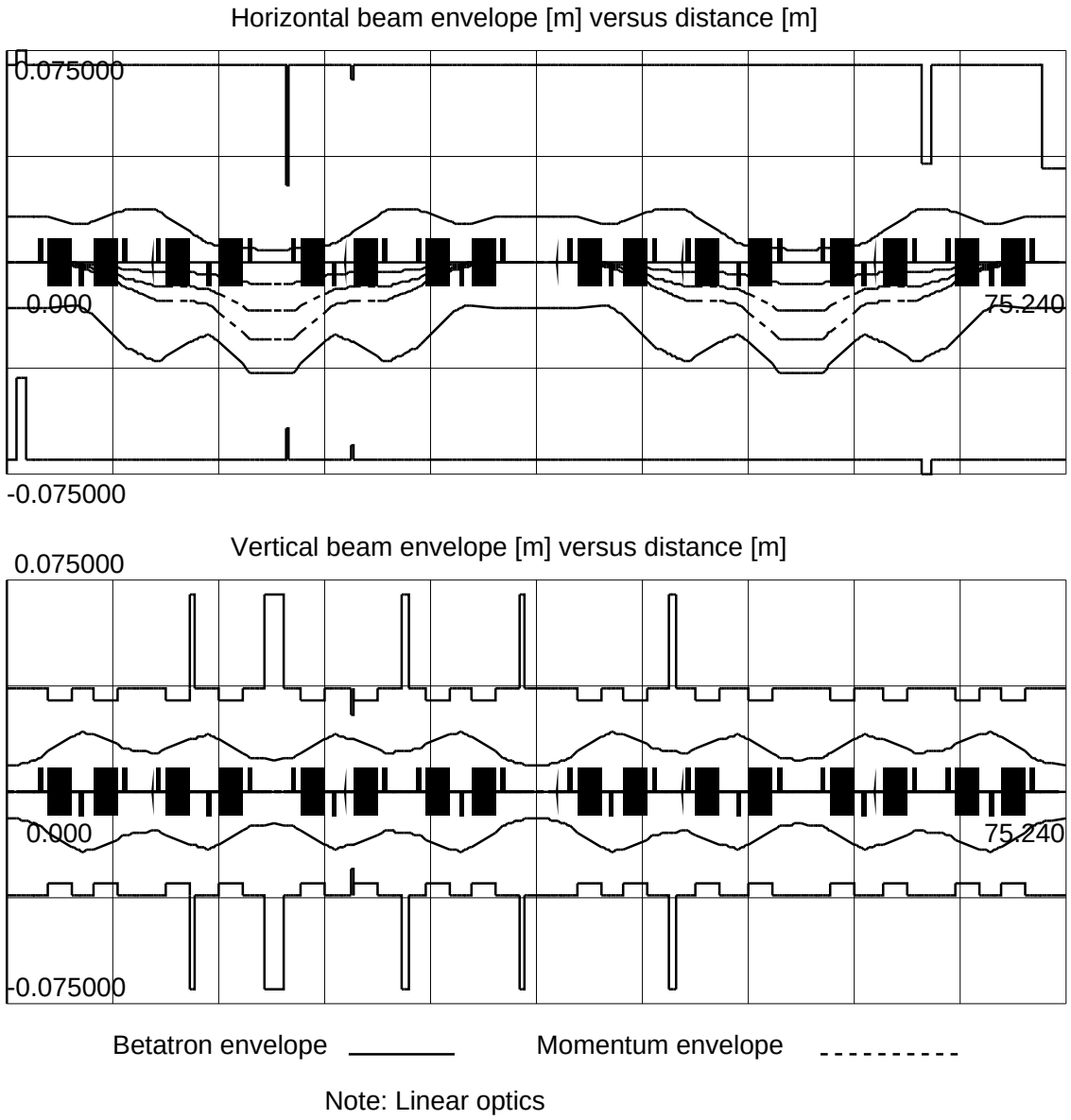

Figure 4: Working hypothesis : horizontal and vertical transverse apertures in PIMMS synchrotron [2], Winagile data. 30 10^{-6} m.rad Carbon optics envelopes including $\delta p/p = \pm 0.0012$ and $< \delta p/p >= -0.0021$ are shown for reference. The lower left obstacle in the horizontal plane is the injection septum, the two upper right ones are the extraction septa.

by the injection and extraction septa. Accordingly, multiturn injection simulations to follow show that the injection septum is responsible for the losses in the first injected turns, whereas magnetic septa are responsible for the losses in the last injected turns.

For the geometrical acceptance calculations two methods are used, either a transport of the main obstacles (transverse apertures of regular optical elements, electrostatic and magnetic septa, exclusive of any scraper limitations), or multiturn multiparticle tracking.

In all cases, assessments are performed with zero momentum spread and zero momentum average.

As a result, the injected beam emittances (Carbon optics : 30 10^{-6} ; proton 20 MeV optics : 12.5 10^{-6} ; proton 7 MeV optics : 21 10^{-6}) appear to fit well within the geometrical acceptance.

Carbon injection optics

Figs. 5,6 show the geometrical acceptance in the Carbon injection optics case, as observed at the electrostatic injection septum. Optics conditions are those given on page 3. Fig. 7 shows the corresponding maximum envelopes with emittances

$$\epsilon_x/\pi = 80\ 10^{-6}\ \text{m.rad},\ \epsilon_z/\pi = 75\ 10^{-6}\ \text{m.rad},$$

given the periodical optical functions $\beta_x = 8.5279, \alpha_x = -0.16248$, $\beta_z = 3.5132, \alpha_z = -0.46866$ at exit of injection septum (left end of the graph).

Proton injection optics, 20 MeV and 7 MeV

Fig. 8 shows the geometrical acceptance in the proton injection optics case, as observed at the electrostatic injection septum. Optics conditions are those given on page 4 with largest tune values upon space-charge induced tune shift, that yield the maximum envelopes with emittances

$$\epsilon_x/\pi = 70\ 10^{-6}\ \text{m.rad},\ \epsilon_z/\pi = 65\ 10^{-6}\ \text{m.rad},$$

shown in Fig. 9 ; the corresponding periodical functions at exit of injection septum (left end of the graph) are $\beta_x = 7.031, \alpha_x = -.1997$, $\beta_z = 3.109, \alpha_z = -.5807$.

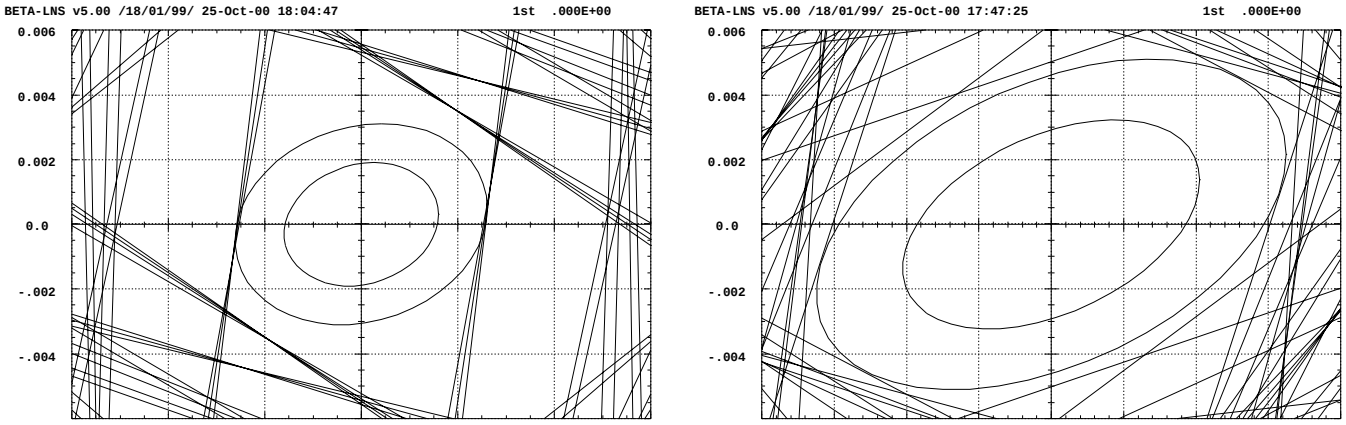

Figure 5: Geometrical acceptance, Carbon case, injection optics. Left : horizontal ; ϵ_x/π = 80 10^{-6} m.rad and ϵ_x/π = 30 10^{-6} m.rad ellipses are superimposed. Right : vertical ; ϵ_z/π = 75 10^{-6} m.rad and $\epsilon_z/\pi = 30\ 10^{-6}$ m.rad are superimposed.

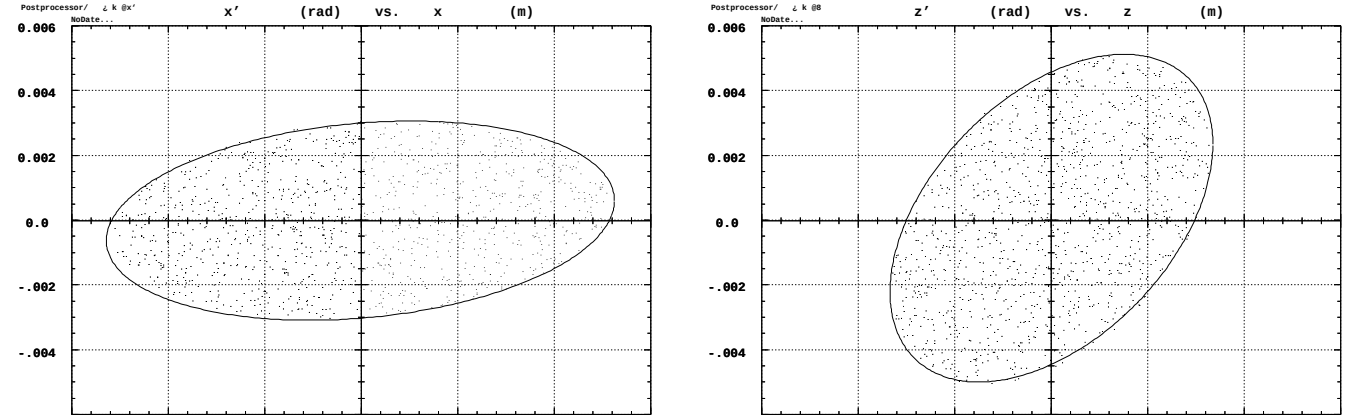

Figure 6: Similar to Fig. 5, from multiturn tracking : final conditions of non-rejected particles after about 40 turns, as observed at exit of injection septum. Matched elliptical borders are for $\epsilon_x/\pi = 79\ 10^{-6}$ m.rad, $\beta_x = 8.74,\ \alpha_x = -0.20$ and $\epsilon_z/\pi = 75\ 10^{-6}$ m.rad, $\beta_z = 3.70,\ \alpha_z = -0.51$.

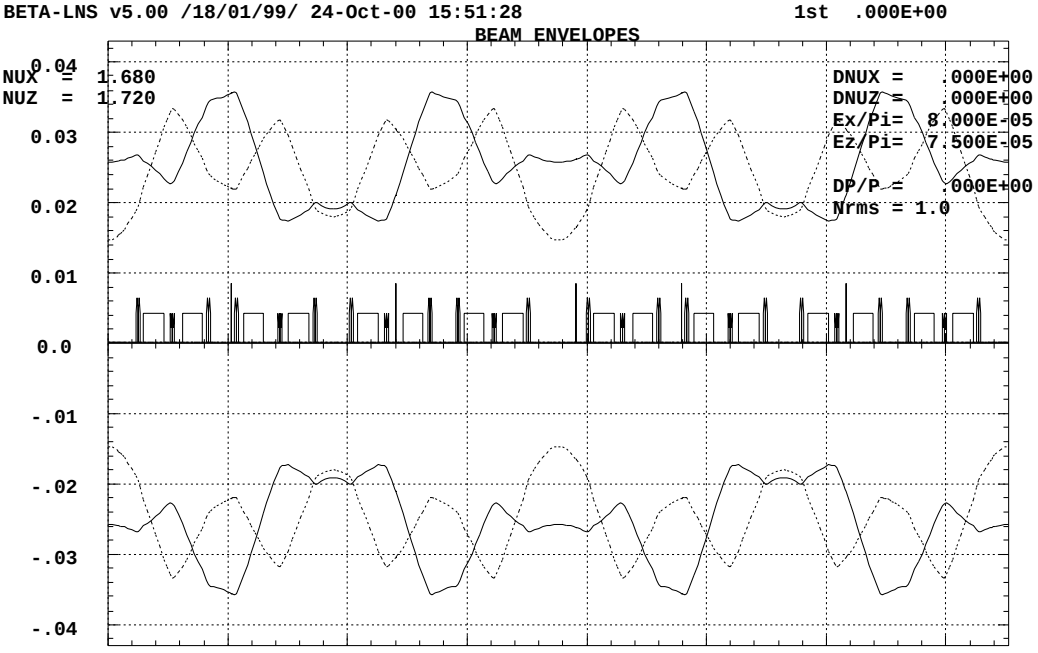

Figure 7: Largest accepted envelopes (on-momentum), Carbon case, injection optics. ϵ_x/π = 80 10^{-6} m.rad, $\epsilon_z/\pi = 75\ 10^{-6}$ m.rad, $\delta p/p \equiv 0$.

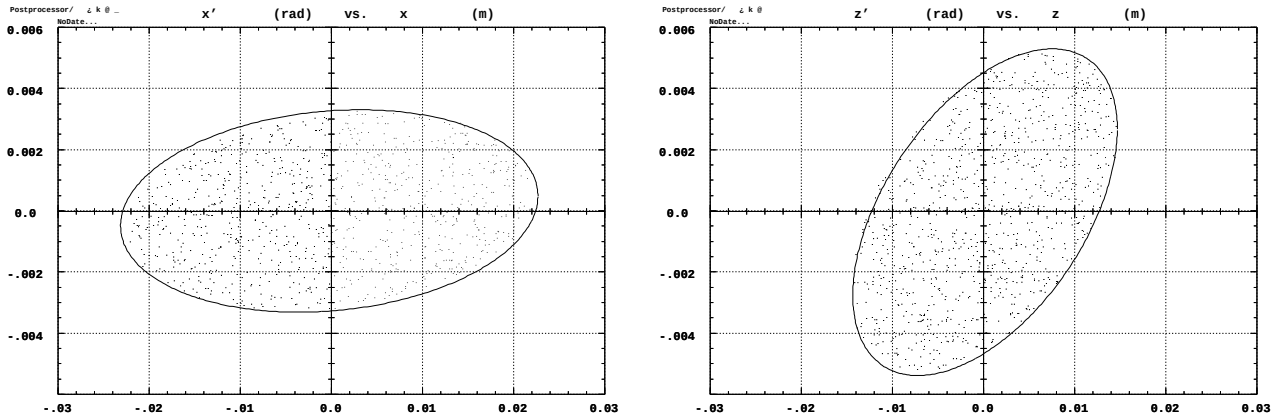

Figure 8: Geometrical acceptance, proton injection optics, 20 MeV and 7 MeV ; phase spaces of non-rejected particles after 50 turns, observed at exit of injection septum. Matched ellipses are for $\epsilon_x/\pi = 72\ 10^{-6}$ m.rad, $\beta_x = 6.98,\ \alpha_x = -0.19$ and $\epsilon_z/\pi = 67\ 10^{-6}$ m.rad, $\beta_z = 3.25,\ \alpha_z = -0.54$.

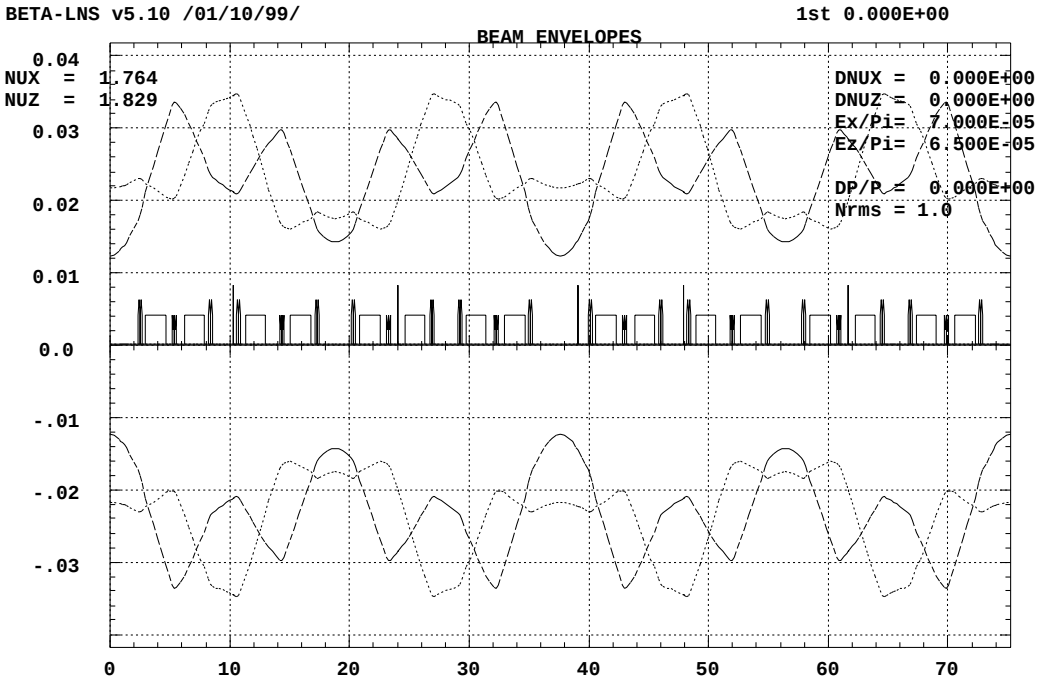

Figure 9: Largest envelopes (on-momentum), proton case, injection optics. $\epsilon_x/\pi = 70\ 10^{-6}$ m.rad, $\epsilon_z/\pi = 65\ 10^{-6}$ m.rad, $\delta p/p \equiv 0$.

3 Review of the injection

Various aspects of the injection reviewed are discussed hereafter ; the list is not exhaustive and presents most significant samples of the work achieved, much more details can be found in written minutes of the Project Technical Group Meetings [8].

This reviewing properties of PIMMS injection will allow in particular designing 7 MeV proton injection, and assessing injection from outwards in straight section SS-21. Apart from these special cases, unless otherwise specified working hypothesis are PIMMS data, in particular typical geometrical conditions are schemed in Fig. 10 that shows the envelope of the first injected turn, after Winagile data.

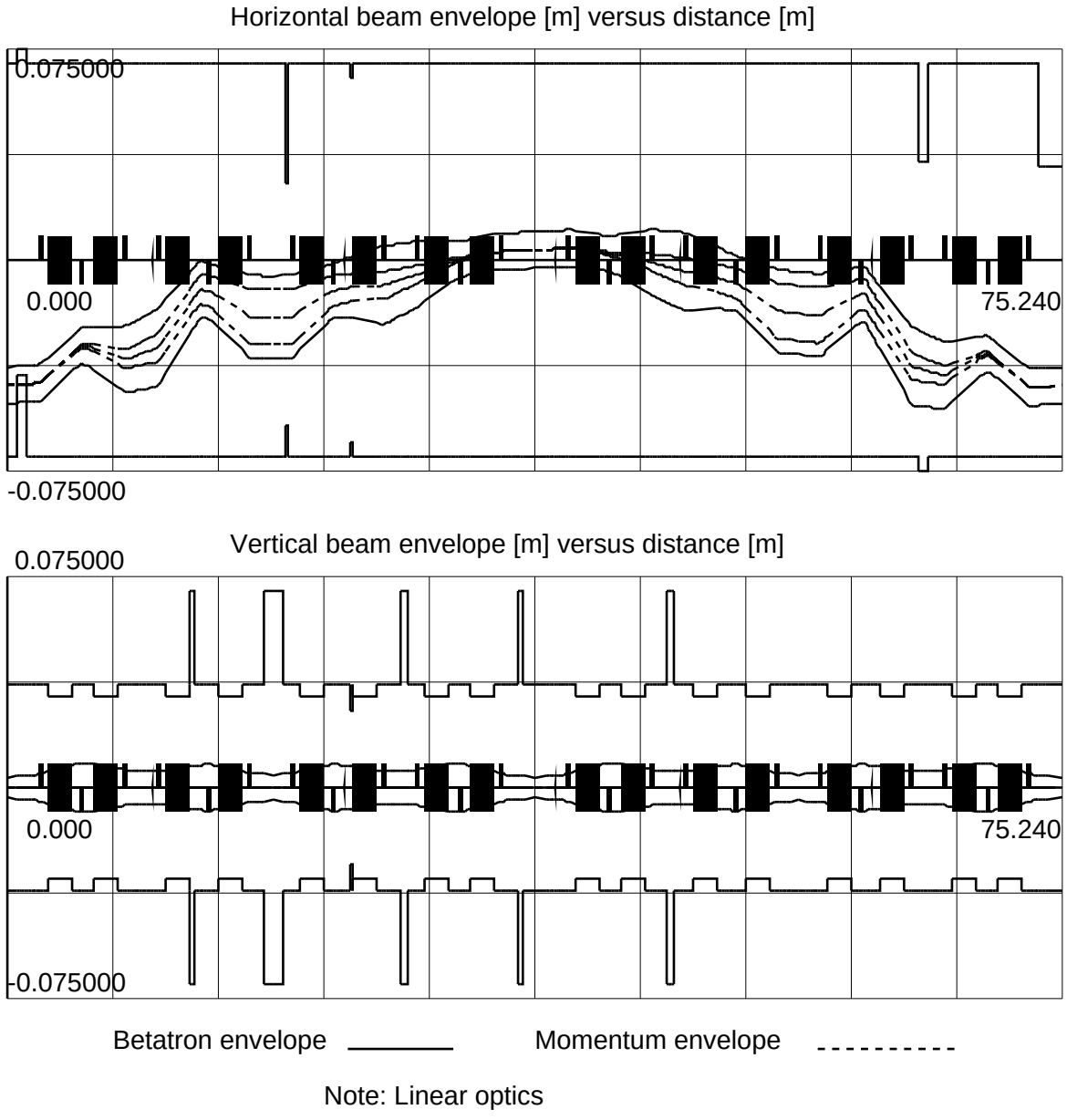

Figure 10: Working hypothesis : horizontal and vertical envelopes of the first injected turn in PIMMS synchrotron [2] (from Winagile) in the hypothesis, for illustration, of Carbon injection optics, 5 10^{-6} m.rad emittances, $\delta p/p = \pm 0.0012$ and $< \delta p/p >= -0.0021$.

Known injection parameters are the emittances to be stored $\epsilon_{x,z}/\pi$, the ring optical functions at the injection azimuth $\alpha_{x,z}, \beta_{x,z}$, and the injected emittances $\epsilon_{x,z,inj}/\pi$.

The horizontal injected ellipse is assumed to be homothetic of the stored one, centered on $x_{co_{inj}}$, $x'_{co_{inj}}$, both values being determined from the position of the injected beam with respect to (close to) the injection septum [2, PartII,Tab.7.5,p.186 (Carbon case)][2, PartII,Tab.7.6,p.188 (proton case)]. On the other hand, given the position of the injection closed orbit bumpers, $x_{co_{inj}}$ determines the closed orbit bump kick (Carbon : -0.0074 rad, proton : -0.0084 rad). The number of turns of the multiturn injection process has a sensible effect on effectiveness and on final transverse uniformity, and can be determined from the previous parameters in the way described in App. A.

The vertical injected ellipse is assumed to be rect so that $\alpha_{z,inj} = 0$, and injected with incidence $z'_{co_{inj}}$ zero. Near-optimum values of the injected ellipse parameter $\beta_{z,inj}$ and position $z_{co_{inj}}$ that warrant final uniformity can be estimated in the way described in App. B.

The simulations that follow show that the vertical motion in the multiturn injection process yields in a natural way the nominal vertical emittance. By contrast the required horizontal emittance is reached in two stages : first the whole geometrical acceptance is filled (yet the last turns are lost, due mostly to the extraction septa), then the beam is scraped[3] down to its nominal horizontal emittance value.

3.1 Carbon, injection into SS-1

Optical conditions

•*Periodic optical conditions at injection azimuth* are the injection septum exit ones, namely (regardless of slight vertical detuning due to residual closed orbit in the chromaticity sextupoles in presence of the injection bump),

$\beta_x = 8.5278$ m, $\alpha_x = -0.1625$, $\beta_z = 3.513$ m, $\alpha_z = -0.4687, \gamma_z = 0.348$

• *Closed orbit coordinates at injection azimuth,* in presence of injection bump induced by -0.0074 rad kicks are

$x_{co_{inj}} = -4.4492\ 10^{-2}$ m, $x'_{co_{inj}} = 7.3752\ 10^{-5}$ rad, $z_{co_{inj}}$ and $z'_{co_{inj}} \equiv 0$

• *Injected beam conditions at injection azimuth are :*

- coordinates wrt. machine axis :

$x_{inj} = -0.0476$ m, $x'_{inj} = -0.0001$ rad, $z_{inj} = -0.0045$ m ($\approx -3\sqrt{\epsilon_z/\pi/\gamma_z}/7 = -3\sqrt{3010^{-6}/0.348}/7 = -0.0040$, according to App. B), $z'_{inj} = 0$;

- beam parameters and emittances :

$\beta_{x,inj} = 8.5278$ m, $\alpha_{x,inj} = -0.1625, \epsilon_{x,inj}/\pi = 5\ 10^{-6}$ m.rad, $\beta_{z,inj} = 5.7$ m ($\approx \frac{16}{49}\frac{1}{\gamma_z}\frac{\epsilon_z}{\epsilon_{z,inj}} = \frac{16}{49}\frac{1}{0.348}\frac{30}{5} = 5.63$, cf. App. B), $\alpha_{z,inj} = 0, \epsilon_{z,inj}/\pi = 5\ 10^{-6}$ m.rad,
$-1.2\ 10^{-3} < \delta p/p < 1.2\ 10^{-3}$ centered on $< \delta p/p >= -0.0021$.

• For practical reasons particle distributions are taken here uniform over 2-D ellipse surface, i.e., elliptic in projection : $\rho(y = x, z) = \sqrt{1 - y^2/a^2}/\pi a$ (whereas PIMMS study considers elliptic 2-D distributions, parabolic 1-D projections, which has no fundamental effect as to our present concern).

A simulation of the fine structure of the dynamics of injection has been performed, including a dynamics model (App. C) ; this is summarized in Figs. 11-12. The spiral form of the arms of the $i = 1, N$ beamlet distribution as observed at turn N (e.g., $N = 16$ in Fig. 12) can be expressed under the form of the phase shift between beamlets $\#i$ and $\#i+k$,

$$\phi_{N,i+k} - \phi_{N,i} = -2\pi k(2/3 + \epsilon) \quad (1)$$

[3] This is supposed to be performed [2, PartII,Sec.7.3,p.183] with either fixed [2, PartII,Fig.M1,p.260] or mobile [2, PartII,Fig.M4,p.262] scrapers.

wherein $\epsilon = \nu_x - int[\nu_x] - 2/3$ (the effects of momentum and amplitude detuning can be included, this is the case in Fig. 12) ; taking $k = 3l$ (l=integer) for the Carbon case one gets $\phi_{N,i+3l} - \phi_{N,i} = -4\pi - 6\pi l\epsilon = -6\pi l\epsilon$ $[2\pi]$ phase shift at turn N between beamlets $\#i$ and $\#i+3l$ that happen to stand on the same arm : in particular these are straight if $\epsilon = 0$ i.e., if $\nu_x = 1+2/3$.

Table 1 shows particle losses, beamlet by beamlet : each one of the i=1, 16 beamlets is launched alone and tracked for the 16-i+1 turns of the multiturn injection process, plus a few additional turns for stabilization of the scraping by the geometrical aperture, the Table gives the number of particles that have survived ; all initial conditions are that of Carbon injection as given above. Finer insight shows that all losses occur in the horizontal plane (this is because the vertical emittance of the stored beam is far less than the geometrical acceptance), the first injected turns loose their particles into the injection electrostatic septum, whereas the last injected turns loose their particles, soon after injection, mostly into the extraction electrostatic and magnetic septa.

Table 1: Single 1000-particle beamlets, 16-turn Carbon injection conditions, 30-turn survival. All beamlets from #12 and beyond are fully lost.

beamlet #	1	2	3	4	5	6	7	8	9	10	11	12	13
Remaining particles	352	702	848	886	922	954	978	944	743	464	233	0	0

Figures 13-15 show the simulation of the full multiturn process followed by beam scraping down to the 30 10^{-6} m.rad nominal emittances, and corresponding x- and z-projected histograms, following PIMMS conditions [2, PartII,Tab.7.5,p.186].

The final emittances after injection are (Fig. 13) $\epsilon_x/\pi \approx 100$ 10^{-6} m.rad, slightly more than the geometrical acceptance (cf. Figs. 5, 6) benefitting from the off-momentum beam centering, and $\epsilon_z/\pi \approx 30$ 10^{-6} m.rad. Agreement with PIMMS data [2, PartII,Fig.7.9,p.186] is satisfying, in particular as to the histograms with FWHH widths (next to scraping, Fig. 14 as to the horizontal histogram) very close to the 24 mm horizontal and 10.8 mm vertical PIMMS values, and as to the injection efficiency (Fig. 15).

Injection efficiency

Accounting for a scraper collimator at appropriate location (where $D_x = 0$) and time (when the closed orbit injection bump is zero in order to avoid residual effects), in order to reduce the horizontal emittance to $\epsilon_x \approx 30$ π mm.mrad, only about 2200 particle over 9600 launched do survive (Fig. 14) (approximately in the ratio of emittances prior to and after scraping : $4650 * 34$ $10^{-6}/80$ $10^{-6} \approx 2000$), hence an efficiency of 23% ; times 16 injected turns this yields 3.7 effective turns, which stands the comparison with the 3.6 PIMMS value [2, PartII,Tab.7.5,p.186].

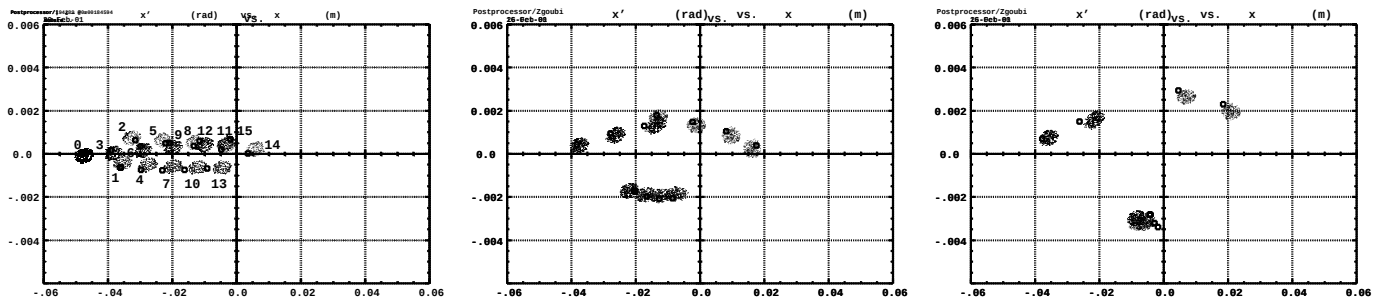

Figure 11: Carbon injection, observation of single beamlets at injection septum. Left : beamlet #2, footprint numbered 0 is the injected beam position, footprints numbered 1 to 15 are the beamlet positions at the end of the corresponding turns ; it can be seen that the beamlet is dragged towards the machine axis while the closed orbit bump collapses. Middle : beamlet #6 (11 footprints). Right : beamlet #10 (7 footprints).
Emittances here are taken very small for better insight, $dp/p \equiv 0$, sextupoles are zero. Superimposed squares are from the geometrical dynamics model and stand the comparison (App. C - amplitude detuning is not accounted for).

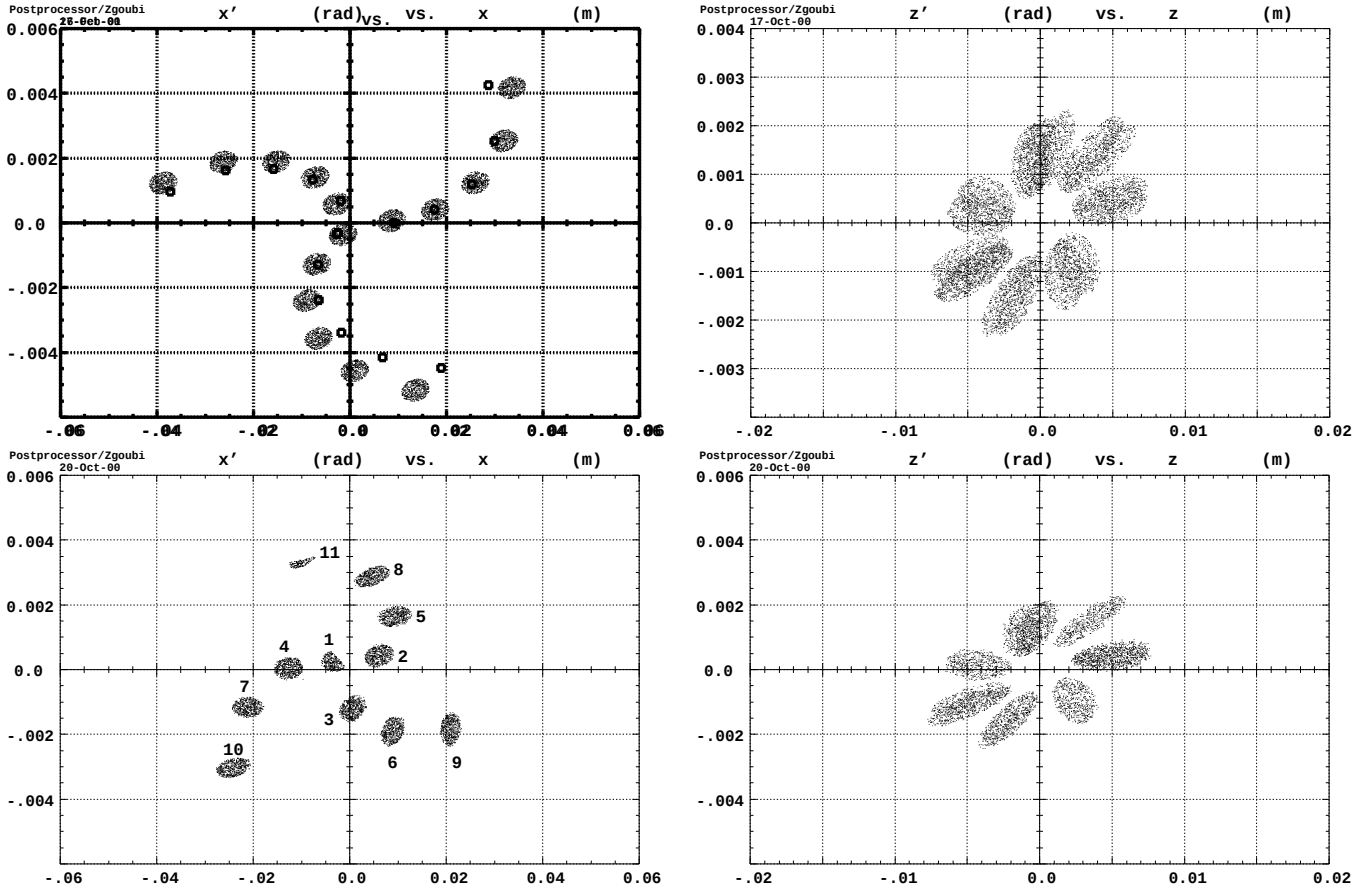

Figure 12: Carbon injection, 16 turns injected, horizontal and vertical phase spaces observed at injection septum at end of turn # 16. Conditions are those in [2, PartII,Tab.7.5,p.186] but for x,z emittances=$10^{-6}\pi$ used for finer insight.
Top row : all sextupoles off, $\delta p/p = 0$, no collimators ; analytical model (squares, accounting for momentum detuning) is superposed in H-phase space. Bottom row : chromaticity sextupoles on, $\delta p/p = 0$ centered on $< \delta p/p >= -0.0021$, collimators set ; beamlet numbers are displayed and show that beamlet #1 (the first injected) is seriously cut (by the injection electrostatic septum, at the end of its third turn around the ring) as well as #11 (cut next to injection, by the extraction magnetic septum) whereas beamlets $\#12 - 16$ are off geometrical acceptance.

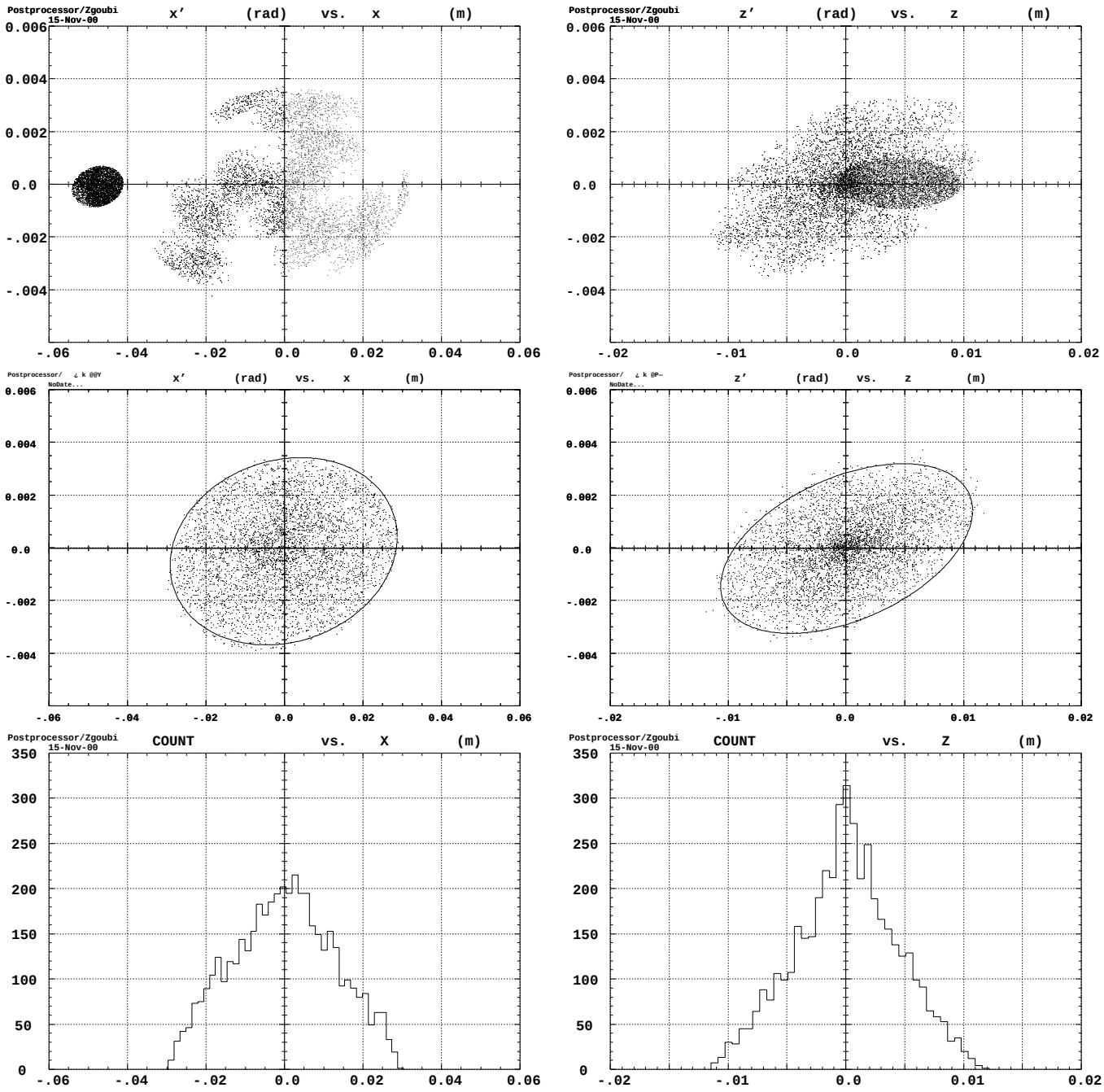

Figure 13: Carbon injection, sextupoles on, 16 turns injected following conditions of [2, PartII,Tab.7.5,p.186] ; $\delta p/p = \pm 1.2\ 10^{-3}$ centered on $< \delta p/p >= -0.0021$ $\epsilon_{x,inj} = \epsilon_{z,inj} = 5\ 10^{-6}\ \pi$. Collimators are set in quads, bends, sextu, injection septum, extraction septa.
Top row : observation at end of turn 16 at injection septum ; the darker spots represent the beam at injection.
Middle and bottom rows : diluted phase spaces after 50 turns, solid ellipses : $\epsilon_x/\pi = 100\ 10^{-6}$ m.rad and $\epsilon_z/\pi = 31\ 10^{-6}$ m.rad borders, and corresponding histograms.

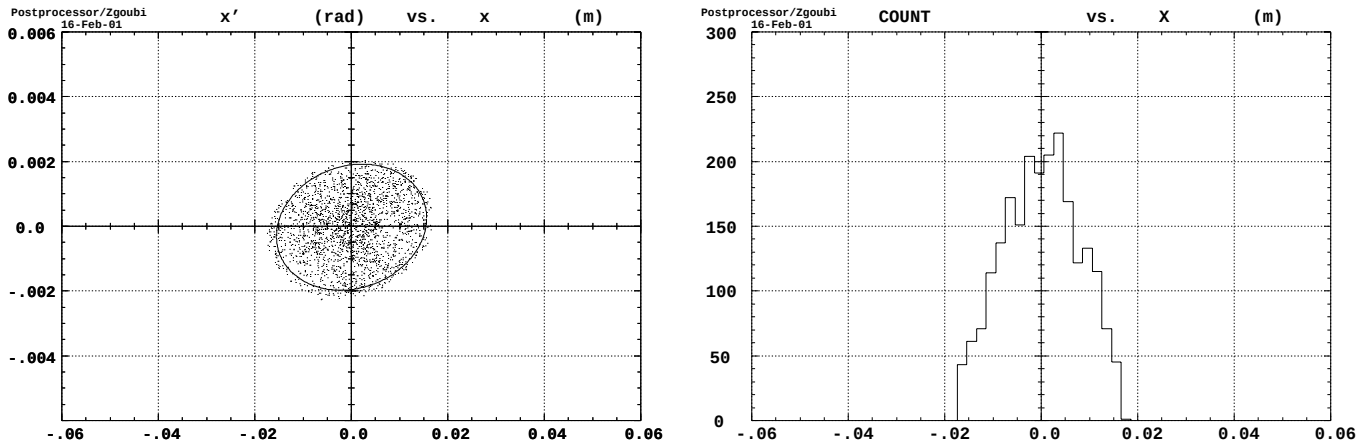

Figure 14: Carbon injection, horizontal emittance after 25-turn scraping using scraper-H located in SS-21. Solid ellipse : the 4-σ statistical limit at 30 10^{-6} m.rad ; 2230 particles over 16×600 injected survive.

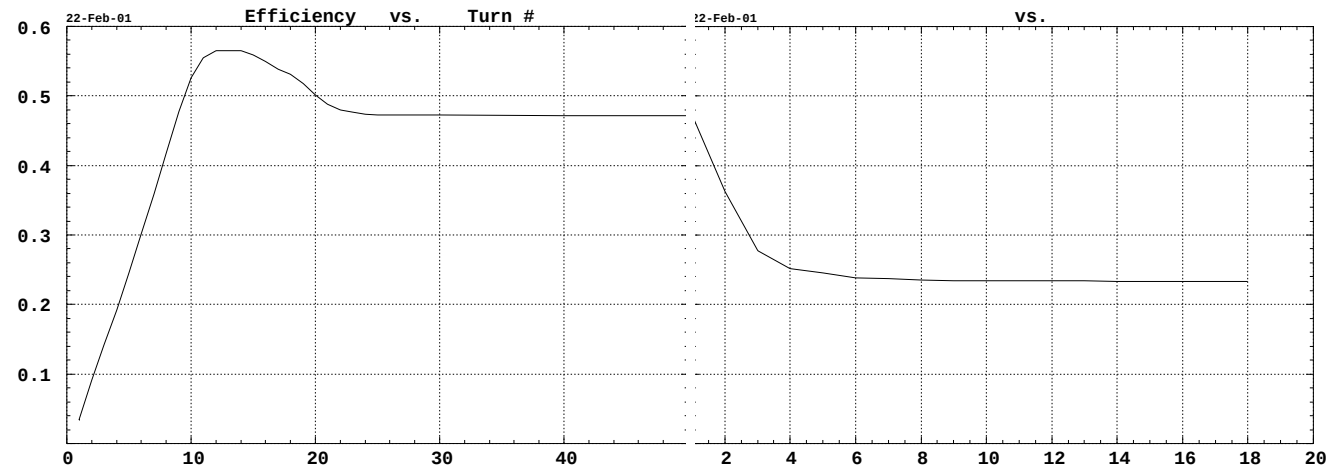

Figure 15: Carbon injection efficiency : relative number of circulating particles (N(turn#)/9600) vs turn #, for 16 injected turns × 600 particles/turn = 9600 particles launched. Prior to scraping (left part of the curve, cf. emittances and hitograms in Fig.13) the efficiency is $\approx 4530/9600 = 47\% \rightarrow \times 16 = 7.5$ effective turns ; after scraping (right part of the curve, cf. Fig.14) the efficiency becomes $23\% \times 16 = 3.7$ effective turns in agreement with 3.6 PIMMS value [2, PartII,Tab.7.5,p.186].

3.2 Proton, injection into SS-1, 20 and 7 MeV

20 MeV

•*Periodic optical conditions at injection azimuth* are the injection septum exit ones, namely (regardless of slight vertical detuning due to residual closed orbit in the chromaticity sextupoles in presence of the injection bump),

$\beta_x = 7.031$ m, $\alpha_x = -0.1997$, $\beta_z = 3.109$ m, $\alpha_z = -0.5807$

• *Closed orbit coordinates at injection azimuth,* in presence of injection bump induced by -0.0084 rad kicks are

$x_{co_{inj}} \approx -5\ 10^{-2}$ m, $x'_{co_{inj}} \approx 0$, $z_{co_{inj}} = z'_{co_{inj}} \equiv 0$

• *Injected beam conditions at injection azimuth are :*

- coordinates wrt. machine axis :

$x_{inj} = -0.0456$ m, $x'_{inj} = -0.0006$ rad, $z_{inj} = -0.0023$ m, ($\approx -3\sqrt{\epsilon_z/\pi/\gamma_z}/7 = -3\sqrt{12.510^{-6}/0.43}/7 = -0.0023$, according to App. B), $z'_{inj} = 0$;

- beam parameters and emittances :

$\beta_{x,inj} = 7.03$ m, $\alpha_{x,inj} = -0.1997$, $\epsilon_{x,inj}/\pi = 3\ 10^{-6}$ m.rad, $\beta_{z,inj} = 3.8$ m ($\approx \frac{16}{49}\frac{1}{\gamma_z}\frac{\epsilon_z}{\epsilon_{z,inj}} = \frac{16}{49}\frac{1}{0.43}\frac{12.5}{3} = 3.2$, cf. App. B), $\alpha_{z,inj} = 0$, $\epsilon_{z,inj}/\pi = 3\ 10^{-6}$ m.rad,
$\delta p/p = \pm 1.2\ 10^{-3}$ centered on $< \delta p/p >= -0.0018$.

• Particle distributions are uniform over 2-D ellipse surface, i.e., elliptic in x and z projections : $\rho(y = x, z) = \sqrt{1 - y^2/a^2}/\pi a$ (not very different from the parabolic ones used in PIMMS).

Figures 16-17 show the simulation of the full multiturn process followed by beam scraping down to the $\approx 12.5\ 10^{-6}$ m.rad nominal emittances, and corresponding x- and z-projected histograms.

The final emittances after injection are (Fig. 16) $\epsilon_x/\pi \approx 80\ 10^{-6}$ m.rad $\approx$ eometrical acceptance (cf. Fig. 8), and $\epsilon_z/\pi \approx 12.5\ 10^{-6}$ m.rad. Agreement with PIMMS data [2, PartII,Fig.7.12,p.188] is satisfying, in particular as to the histograms and FWHH widths (next to scraping, Fig. 17) close to the 15.4 mm horizontal and 6.5 mm vertical PIMMS values, and as to the injection efficiency (Fig. 17) : 3.1 effective turns to compare with 3.3 in [2, PartII,Tab.7.6,p.188].

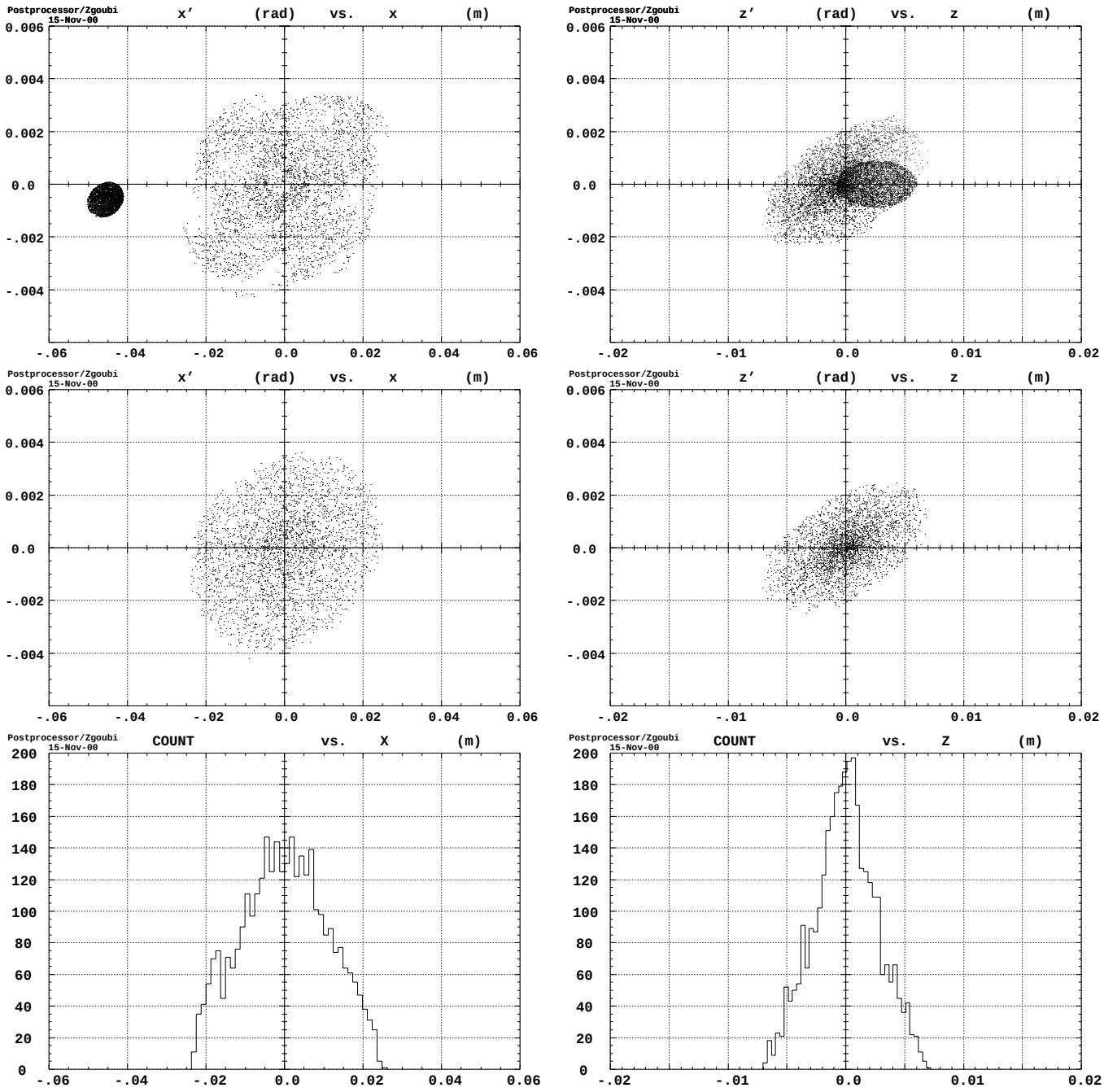

Figure 16: Proton injection, sextupoles on, 28 turns injected following conditions of [2, PartII,Tab.7.6,p.188] ; $\delta p/p = \pm 1.2\ 10^{-3}$ centered on $< \delta p/p >= -0.0018$ $\epsilon_{x,inj} = \epsilon_{z,inj} = 3\ 10^{-6}\ \pi$. Collimators are set in quads, bends, sextu, injection septum, extraction septa.
Top row : observation at end of turn 28 at injection injection septum ; the darker spots represent the beam at injection.
Middle and bottom rows : diluted phase spaces and histograms after 100 turns ; stored emittances are $\epsilon_x/\pi = .024^2/7.03 = 80\ 10^{-6}$ and $\epsilon_z/\pi = .0065^2/3.11 = 13\ 10^{-6}$.

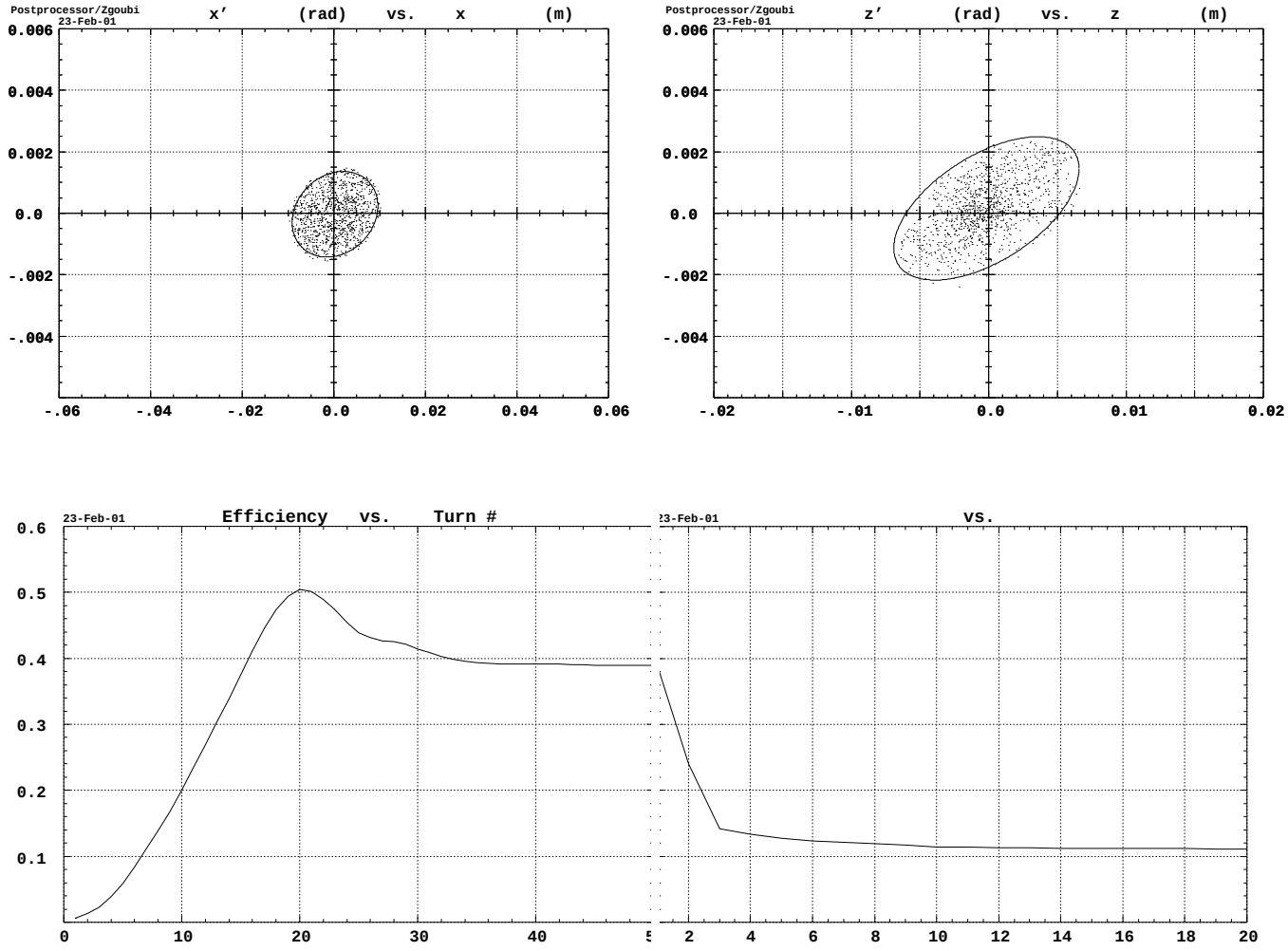

Figure 17: Top : after horizontal scraping, solid elliptical borders : 12.8π x- and 13.0π z-emittance as observed at injection septum.
Bottom : proton injection efficiency, 20 MeV : relative number of circulating particles (N(turn#)/9800) vs turn #, for 28 turns × 350 particles/turn = 9800 particles launched. Left : no scrapers set, efficiency is 28 turns×38.9% = 10.9 effective turns (cf. emittances in Fig. 16) ; right : after 20-turn H-scraping down to 12.5π mm.mrad (# particles : 3814→1091) efficiency is 28 turns×11.1% = 3.1 effective turns (3.3 in [2, PartII,Tab.7.6,p.188]).

7 MeV

The following describes a tentative 7 MeV injection scheme with injected and stored emittances taken in the ratio of the rigidities wrt. the 20 MeV case, $\beta\gamma|_{20\ MeV}/\beta\gamma|_{7\ MeV} = 1.696$. Given that the stored intensity is to be about half the 20 MeV one [7], the space-charge tune shift is almost the same - in fact slightly smaller which is favorable, yet we choose to neglected the difference and maintain the 20 MeV optics for simplicity ; this entails injection simulation with identical ring optics conditions (page 4).

• *Periodic optical conditions at injection azimuth* are the injection septum exit ones, namely (regardless of slight vertical detuning induced by residual closed orbit in the chromaticity sextupoles in presence of the injection bump),

$\beta_x = 7.03$ m, $\alpha_x = -0.1997$, $\beta_z = 3.11$ m, $\alpha_z = -0.581, \gamma_z = 0.430$

• *Closed orbit coordinates at injection azimuth,* in presence of horizontal injection bump induced by -0.0084 rad kicks are

$x_{co_{inj}} \approx -5\ 10^{-2}$ m, $x'_{co_{inj}} \approx 0$, $z_{co_{inj}} = z'_{co_{inj}} \equiv 0$

• *Injected beam conditions at injection azimuth are :*

- coordinates wrt. machine axis :

$x_{inj} = -0.048$ m, $x'_{inj} = 0$ rad, $z_{inj} = \frac{3}{7}\sqrt{\frac{\epsilon_z/\pi}{\gamma_z}} = \frac{3}{7}\sqrt{\frac{1.7\times 12.5\ 10^{-6}}{0.430}} = 0.003$ m with 1.7 being the ratio of 20 MeV to 7 MeV rigidities (cf. App. B), $z'_{inj} = 0$;

- beam parameters and emittances :

injected as well as stored emittances are taken in the ratio of the rigidities wrt. the 20 MeV earlier case ($\beta\gamma|_{20\ MeV}/\beta\gamma|_{7\ MeV} = 1.696$), from what ensues, $\epsilon_{x,inj}/\pi = 1.7 \times 3\ 10^{-6} = 5.1$ m.rad, $\beta_{z,inj} = \frac{16}{49}\frac{1}{\gamma_z}\frac{\epsilon_z}{\epsilon_{z,inj}} = \frac{16}{49}\frac{1}{0.43}\frac{12.5}{3} = 3.2$ m (cf. App. B), $\alpha_{z,inj} = 0$, $\epsilon_{z,inj}/\pi = 1.7 \times 3\ 10^{-6} = 5.1\ 10^{-6}$ m.rad,
$\delta p/p = \pm 1.7 \times 1.2\ 10^{-3} = \pm 2$ centered on $< \delta p/p >= -0.0018$.

- $M = \left(1 + \frac{X_{ESept}}{\sqrt{\beta_x \epsilon_{x,inj}/\pi}}\right)\frac{n}{a}$ =20-turn injection (taking $X_{ESept} = 41$ mm, $n = 4$, $a = 1.5$, according to App. A).

• Particle distributions are uniform over 2-D ellipse surface, i.e., elliptic in projection : $\rho(y = x, z) = \sqrt{1 - y^2/a^2}/\pi a$.

Figure 18 shows the full simulation of the multiturn process followed by beam scraping down to the $\approx 21\ 10^{-6}$ m.rad nominal emittances, and corresponding x- and z-projected histograms.

The final emittances after injection are $\epsilon_x/\pi \approx 100\ 10^{-6}$ m.rad (i.e., slightly more than the geometrical acceptance, benefitting from the off-momentum beam centering) and $\epsilon_z/\pi \approx 21\ 10^{-6}$ m.rad. 20 turns $\times$ 500 particles/turn = 10000 particles have been launched ; prior to scraping, the efficiency is 3377/10000= 33.77% $\rightarrow \times 20$ turns = 6.8 effective turns ; after 20-turn H-scrap down to 21 mm.mrad the efficiency decreases to 1101/9600 = 11.0% $\rightarrow \times 20 = 2.02$ effective turns over 20 which is close to 20 MeV case efficiency of 11.1% = 3.1 effective turns over 28 (page 16).

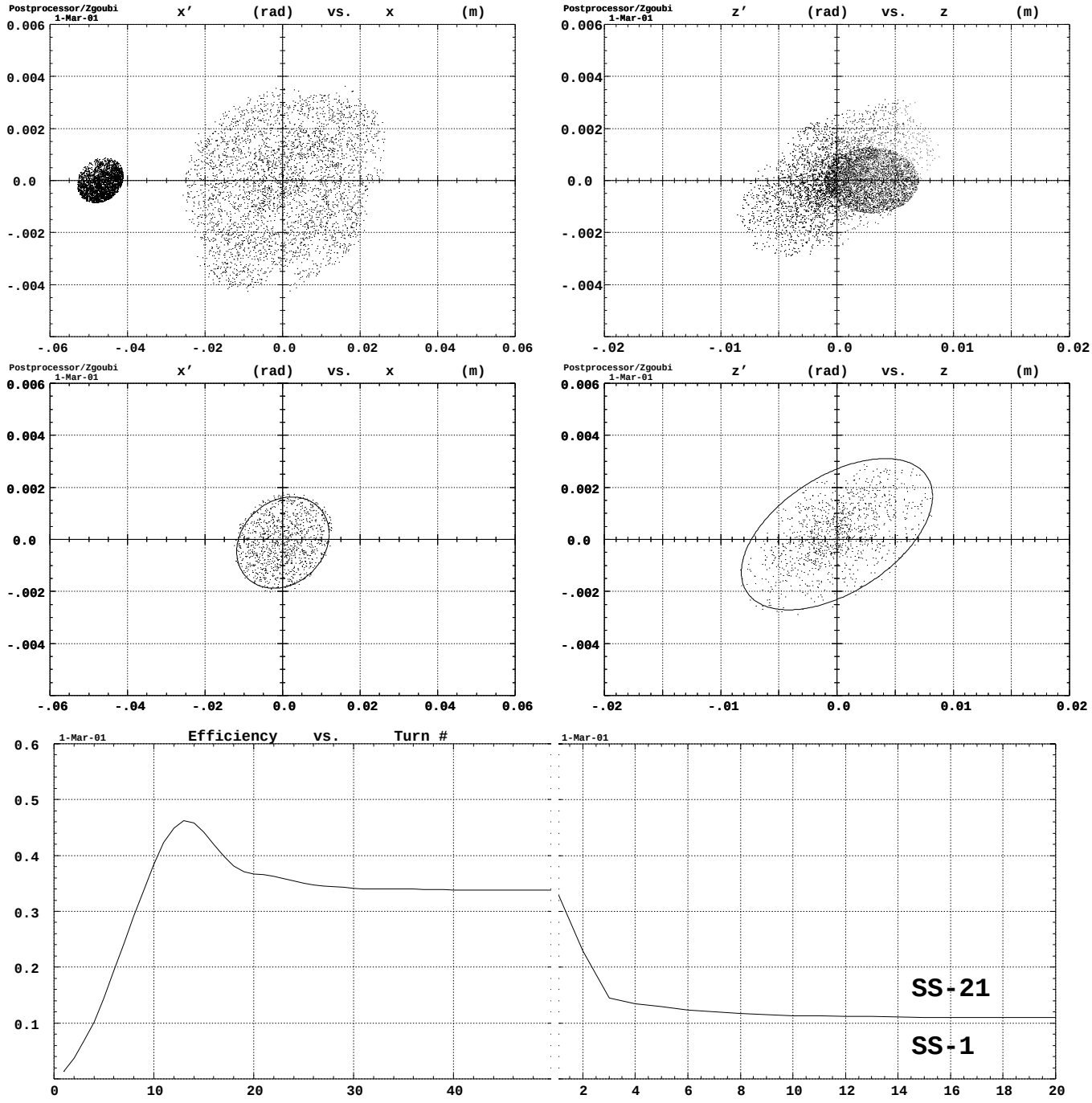

Figure 18: Proton injection, 7 MeV, 20 turns injected. $\delta p/p = \pm 2\ 10^{-3}$ centered on $< \delta p/p >= -0.0018$, $\epsilon_x = \epsilon_z = 5.1\ 10^{-6}\ \pi$. Collimators are set in quads, bends, sextu, injection septum, extraction septa.
Top row : observation at turn 20 at injection septum, $\epsilon_x/\pi \approx 100\ 10^{-6}$ m.rad, $\epsilon_z/\pi \approx 21\ 10^{-6}$ m.rad.
Middle row : phase space at injection septum after 20-turn H-scraping ; solid ellipses have $\epsilon_{x,z}/\pi \approx 20.5\ 10^{-6}$ m.rad.
Bottom row : injection efficiency, left : no scrapers set, 3377 particles over 10000 survive ; right : after 20-turn H-scraping down to 21 mm.mrad, efficiency is $1101/9600 = 11.0\% \rightarrow \times 20$ turns $= 2.02$ effective turns over 20 injected.

4 Injection in straight section 21, from outwards

It can be thought of injecting into PIMMS from outwards at section SS-21, in order to shorten the injection beam line or for installation purposes. This alternative is addressed in the following.

In addition to the layout modifications discussed in Section 4.1 the electrostatic septum and the injection closed orbit bump are now in $x > 0$ regions ; Fig. 19 shows typical 20-turn closed orbit damping for illustration.

The geometry is for the rest similar to the SS-1 case (Fig. 10 page 10).

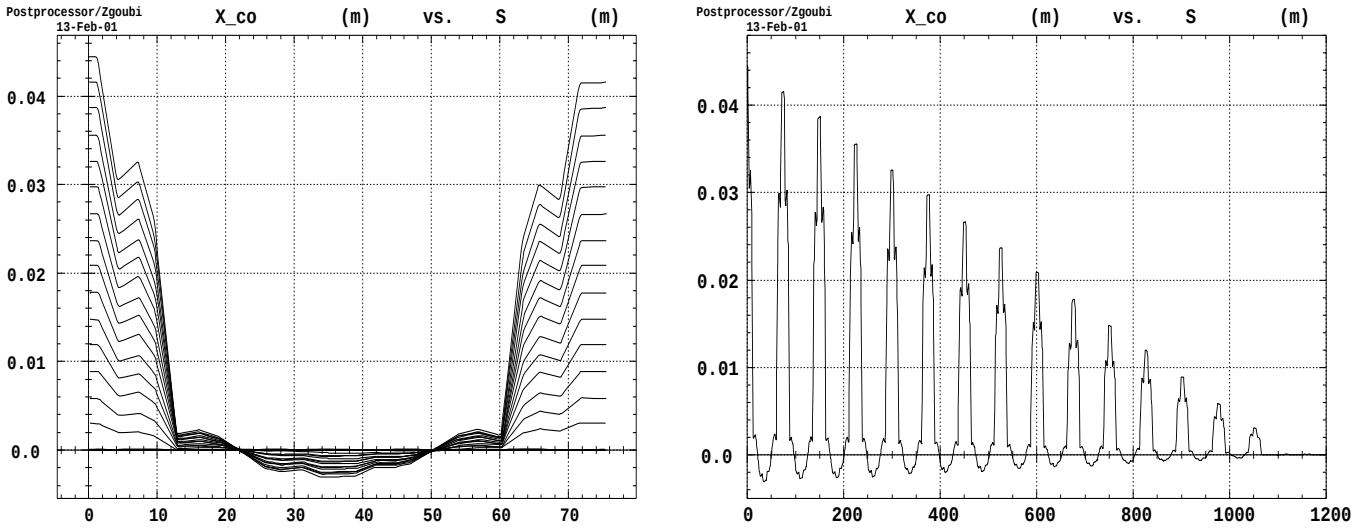

Figure 19: 16-turn injection bump closed orbit damping, Carbon injection into SS-21, sextupoles are off.

4.1 Layout modifications for injection into SS-21

The injection into the ring can be installed in SS-21 by permuting the RF cavity and the electrostatic septum tank (Fig. 20). Yet this entails moving to alternate locations, on the one hand the skew-quad and the h-scraper placed downstream of the RF cavity, and on the other hand the scintillator screen and the dipole corrector placed downstream of the E-septum. Overlapping of the extraction line with the RF tank and of the injection line with three other pieces of equipment also ensue from a crude permutation.

Obviously such change would not go without some re-designing and adjustment of the optics, and in particular re-positioning of the extraction elements.

We choose to forget these aspects for the moment and study in the following, injection in SS-21 in the hypothesis of unchanged optics.

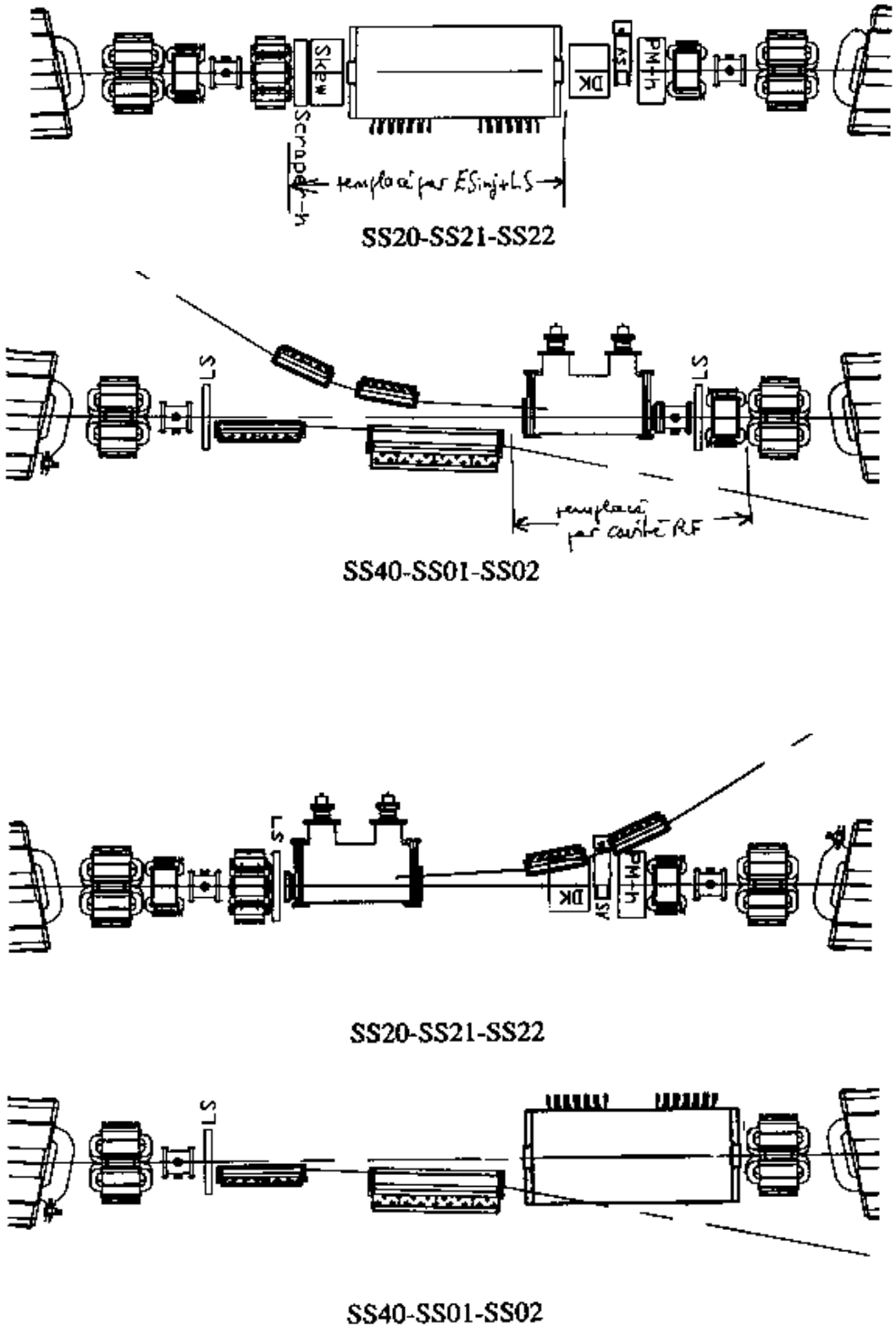

Figure 20: Layout modifications for external injection. Upper two drawings : straight sections SS-21 and SS-1 respectively, prior to modifications ; lower two drawings : after implementation of injection in SS-21 and RF in SS-1.

4.2 Carbon, injection in SS-21

Optical conditions

These are identical to the SS-1 injection case, apart from what follows.

•*Periodic optical conditions at injection azimuth* are the injection septum exit ones, namely $\beta_x = 8.53$ m, $\alpha_x = -0.148$, $\beta_z = 3.47$ m, $\alpha_z = -0.418$, $\gamma_z = 0.339$

•*Optimized parameters are* (after App. B)

$\beta_{z,inj} = 16\epsilon_z$ / $49\gamma_{z,inj}\epsilon_{z,inj} = 16 \times 30\ 10^{-6}$ / $49 \times 0.339 \times 5\ 10^{-6} \approx 5.8$ m ; $z_{inj} = 3\sqrt{\epsilon_z/\gamma_z}/7 = 0.004$ m ; simulations below are realized in fact with slightly different values $\beta_{z,inj} = 5.7$ m, $z_{inj} = 0.0045$ m).

A simulation of the 16-turn injection bump closed orbit damping is shown in Fig. 19. Fig. 21 shows fine structure features of the dynamics of injection including the geometrical model after App. C.

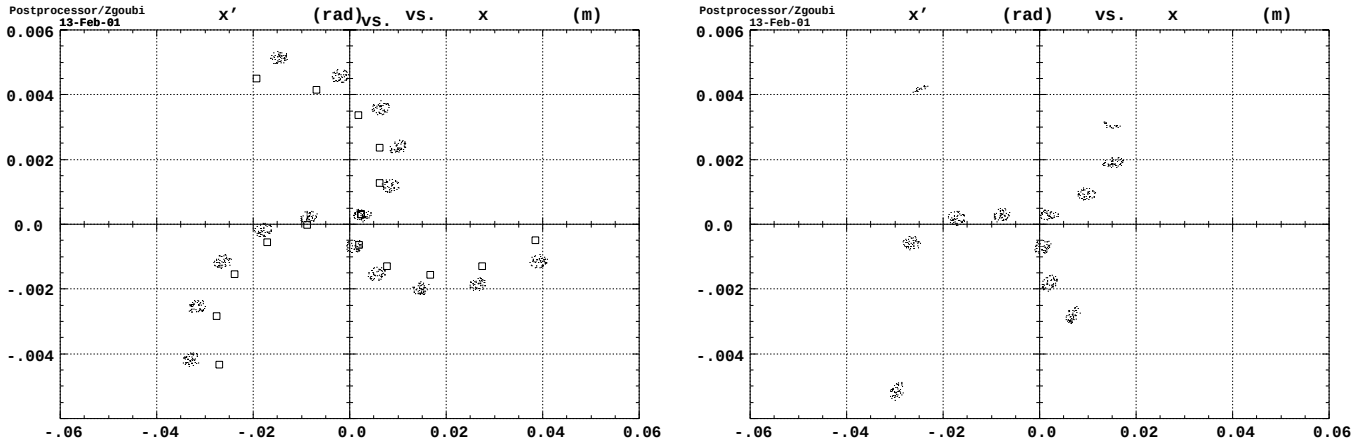

Figure 21: Carbon injection into SS-21, 16 turns injected, H phase space observed at injection septum at end of turn 16. Left : all sextupoles off, $\delta p/p = 0$, no collimators, squares are from analytical model (App. C) ; right : chromaticity sextupoles on, $\delta p/p = 0$ centered on $< \delta p/p >= -0.0021$, collimators set - beamlets $\#11 - 14$ are lost, beamlets #15 and 16 (the outer ones on the right plot) will only survive 3 turns.

Fig. 22 shows a full simulation of the multiturn process followed by beam scraping down to the 30 10^{-6} m.rad nominal emittances.

The stored emittances after injection are $\epsilon_x/\pi \approx 85\ 10^{-6}$ m.rad $\approx$ geometrical acceptance, and $\epsilon_z/\pi \approx 29\ 10^{-6}$ m.rad. 16 turns $\times$ 600 particles/turn = 96000 particles have been launched ; prior to scraping, the efficiency is 44% about 3% less than with injection into SS-1 (cf Fig. 15) ; after 20-turn H-scrap down to 21 mm.mrad the efficiency decreases to 16% $\rightarrow \times 16$ that yields 2.7 effective turns (against 3.6 when injecting into SS-1).

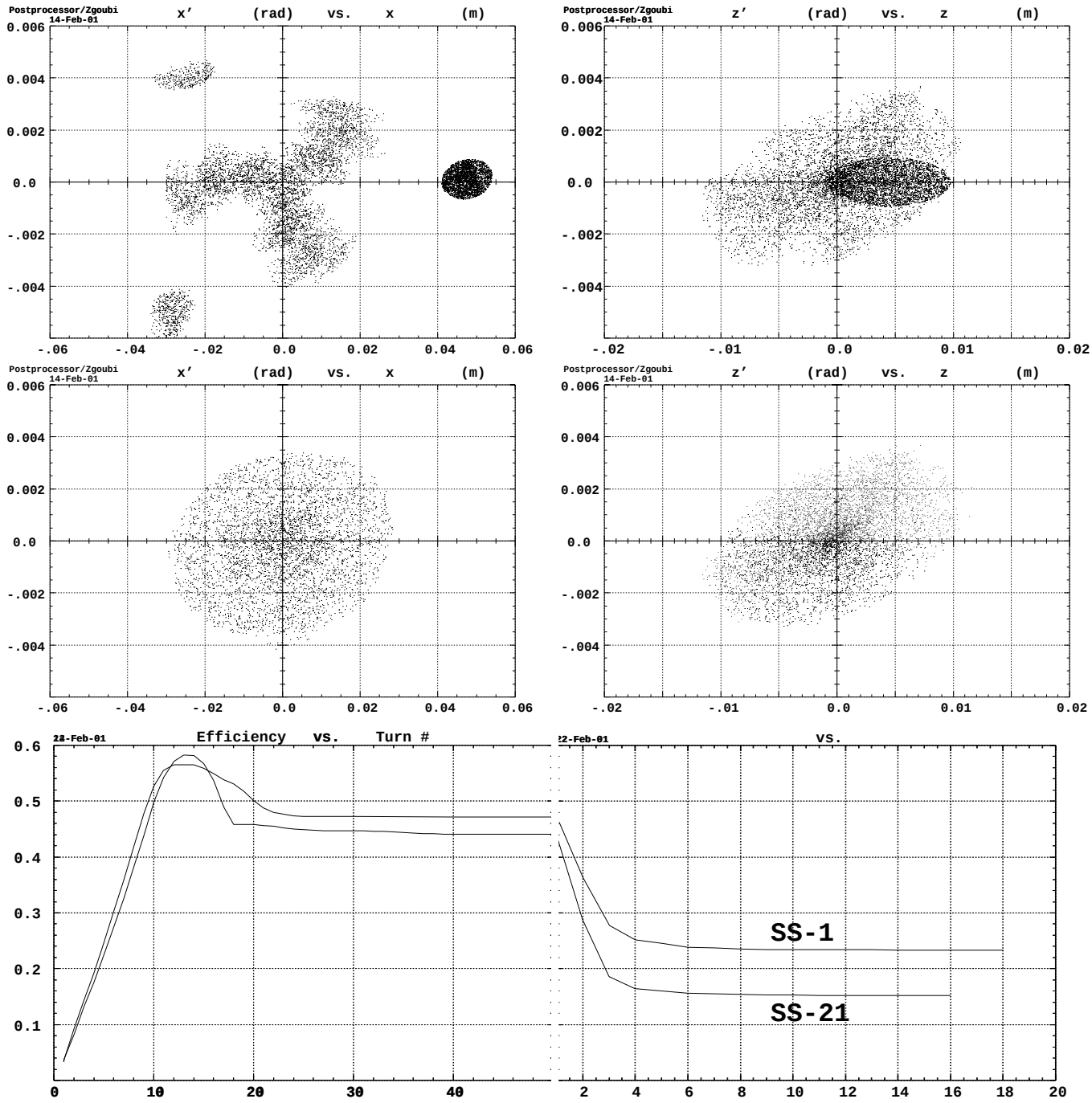

Figure 22: Carbon injection into SS-21, sextupoles on, 16 turns injected ; $\delta p/p = \pm 1.2\ 10^{-3}$ centered on $< \delta p/p >= -0.0021$ $\epsilon_x = \epsilon_z = 5\ 10^{-6}\ \pi$. Collimators are set in quads, bends, sextu, injection septum, extraction septa.
Top row : observation at end of turn 16 at injection septum ; the darker spots represent the beam at injection.
Middle row : diluted phase spaces after 50 turns, limits are at $\epsilon_x/\pi = \sigma_x^2/\beta_x = 0.027^2/8.53 \approx 85\ 10^{-6}$ m.rad and $\epsilon_z/\pi = \sigma_z^2/\beta_z = 0.012^2/3.47 \approx 29\ 10^{-6}$ m.rad.
Bottom row : injection efficiency, worse than in the SS-1 case (Fig. 15, superimposed for comparison) ; the right part of the curve shows the effect of x-scraping down to $30\ 10^{-6}\ \pi$ m.rad that results in 2.7 effective turns.

4.3 Proton, 7MeV, injection in SS-21

Optical conditions

These are identical to the SS-1 injection case, apart from what follows.
•*Periodic optical conditions at injection azimuth* are the injection septum exit ones, namely $\beta_x = 7.0$ m, $\alpha_x = -0.183$, $\beta_z = 3.07$ m, $\alpha_z = -0.50$, $\gamma_z = 0.41$
•*Optimized parameters after App. B* are
$\beta_{z,inj} = \frac{16}{49}\frac{1}{\gamma_z}\frac{\epsilon_z}{\epsilon_{z,inj}} = \frac{16}{49}\frac{1}{0.408}\frac{21.2}{5.1} = 3.3$ m ; $z_{inj} = \frac{3}{7}\sqrt{\frac{\epsilon_z/\pi}{\gamma_z}} == \frac{3}{7}\sqrt{\frac{1.7\times 12.5\ 10^{-6}}{0.408}} = 0.0031$ m.
The optimum injection number of turns is $M = \left(1 + \frac{X_{ESept}}{\sqrt{\beta_x \epsilon_{x,inj}/\pi}}\right)\frac{n}{a}$ =20 (taking X_{ESept} = 41 mm, $n = 4$, $a = 1.5$, according to App. A).

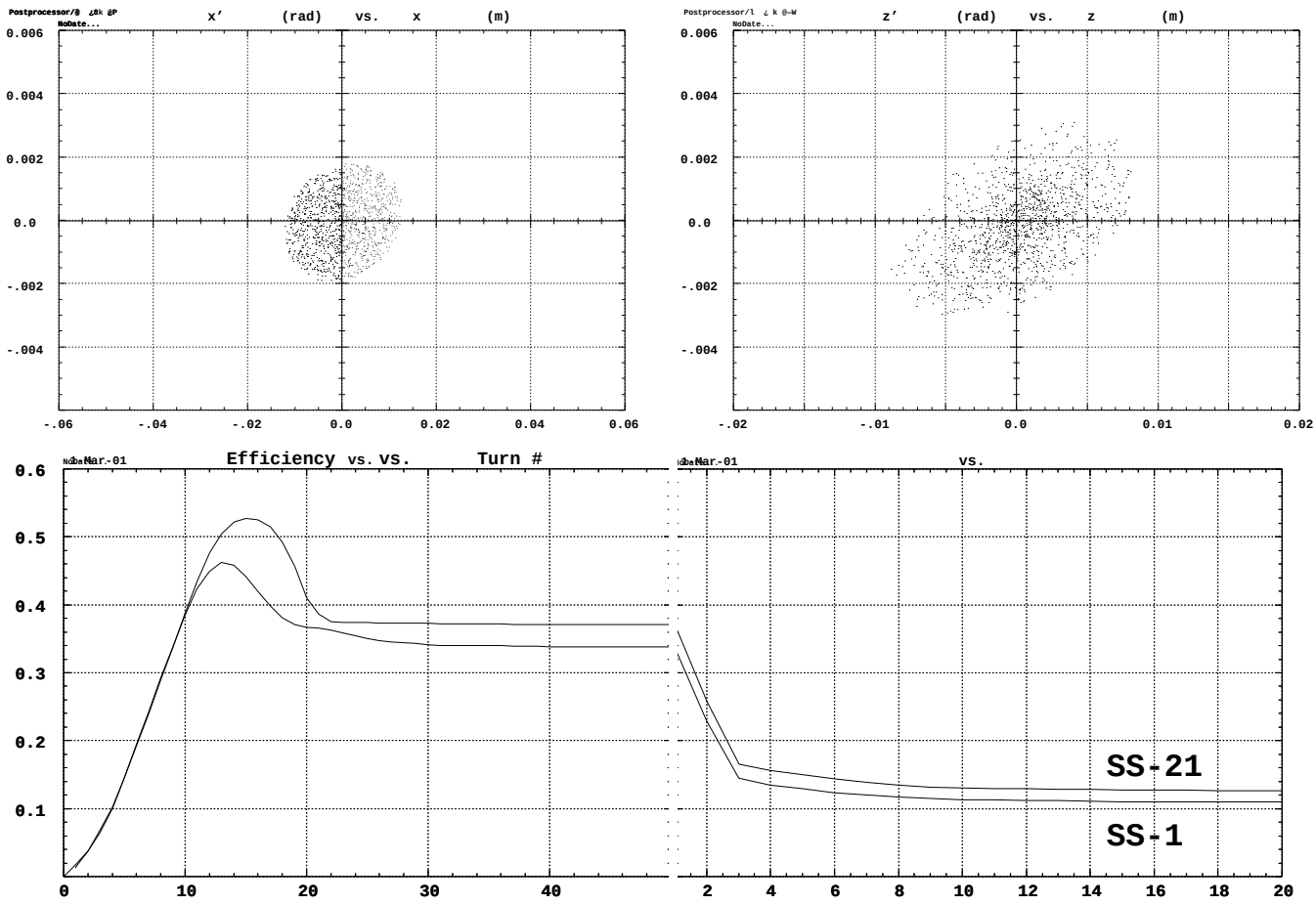

Figure 23: 20-turn 7 MeV proton injection into SS-21 ; $\delta p/p = \pm 2\ 10^{-3}$ centered on $< \delta p/p >= -0.0018$ $\epsilon_x = \epsilon_z = 5.1\ 10^{-6}$ π. Collimators set in quads, bends, sextu, injection septum, extraction septa.
Top row : phase space at injection septum after 20-turn H-scraping down to ≈ 21 mm.mrad ; 10000 particles have been launched. Bottom row : injection efficiency, better than in the SS-1 injection case (Fig. 18, superimposed for comparison) ; left part of the curve : no scrapers set, efficiency = 3700/10000= 37% ; right : after 20-turn x-scrap down to ≈ 21 mm.mrad → efficiency= 1267/10000 = 12.7% → × 20 yields 2.5 effective turns (about 75% the SS-1 20 MeV case, see Fig. 17).

5 A summary of beam emittances and intensities

Table 2 summarises the injected and stored beam emittances and intensities derived in the present study, regarding the Lyon project.

Table 2: Beam emittances and intensities, injected and stored.

		proton		**Carbon**
		1st con's set		
Kinetic energy	MeV	7	20	7
Injected beam				
$\epsilon_{x,z}/\pi$, total	10^{-6}m.rad	5.1	3	5
$\delta p/p$, rms	10^{-3}	± 2	± 1.2	± 1.2
Intensity, SS-1 case	emA	1.38	1.51	0.105
Intensity, SS-21 case	emA	1.12	-	0.143
Stored beam				
$\epsilon_{x,z}/\pi$, total	10^{-6}m.rad	21	12.5	30
Intensity	emA	2.65	4.44	0.368
$< \delta p/p >$		-0.0018	-0.0018	-0.0021

Tables 4, 5 provide beam intensities and particle numbers from source to patient as drawn from the above studies, with that specificity of the Lyon project that the number of protons at patient in the passive spreading case is taken equal to 10^{10} [7] whereas it is $2\ 10^{10}$ in PIMMS case as appears in Table 3 [2, PartII,Tab.7.8,p.192] given for comparison.

The following rules link the various parameters in a Table :

Particles stored = Particles at patient $\times \begin{cases} 3.42 & \text{for proton, passive spreading} \\ 1.98 & \text{for Carbon} \end{cases}$,

Stored current = Particles stored $\times$ Particle charge / Revolution time,

Particles to inject = Particles at patient $\times \begin{cases} 3.6 & \text{for proton, passive spreading} \\ 2.08 & \text{for Carbon} \end{cases}$,

Current in transfer line = Particles to inject $\times$ Particle charge / (Effective turns $\times$ Revolution time),

Filling time = Revolution time $\times$ Injection turns,

Current from source = Current in transfer line / $\begin{cases} 0.585 & \text{for proton, passive spreading} \\ \frac{4}{6}0.558 & \text{for Carbon} \end{cases}$.

In these relations the numerical coefficients are derived from transmission efficiencies as drawn from [2, PartII,Tab.1.6,p.8] for protons and from [2, PartII,Tab.1.7,p.8] for Carbon. Note also that the 3.42 and 3.6 coefficients of the 20 MeV proton case are supposed to apply as well to the 7 MeV proton injection, which may be argued about.

6 Conclusions

The review of Carbon and proton multiturn injection in PIMMS after the CERN documentation has allowed us to show that 7 MeV proton injection with half the intensity of the 20 MeV original PIMMS case, is doable with no important change in the injection optics. It also allowed us investigating a 16-turn 7 MeV Carbon injection and 20-turn 7 MeV proton injection scheme into straight section #21 from outward whereas PIMMS injects from inward into section #1 ; a brute move of the extraction electrostatic septum to the opposite straight section (by permutation with the RF cavity) appears only possible at the price of a slight lengthening (about a meter) of these straight sections, which would necessitate a re-adjustment of machine parameters and in particular of the extraction parameters.

Table 3: For reference : beam intensities, PIMMS case, first set of proton injection conditions after [2, PartII,Tab.1.6,p.8], Carbon and second set of proton injection conditions after Ref. [2, PartII,Tab.7.8,p.192], and

		proton passive spreading		**Carbon**
		1st con's set	2nd con's set	
Nominal energy	MeV/u	20		7
Particles at patient		$2\ 10^{10}$		$4\ 10^{8}$
Particles stored[a]		$6.84\ 10^{10}$		$7.9\ 10^{8}$
Stored current[a]	emA	8.87		0.368
Particles to inject[b] (H^+/C^{6+})		7.2		$8.31\ 10^{8}$
Revolution time	10^{-6}s	1.235		2.058
Injection turns		28		16
Effective turns		3.3	3.1	3.6
Filling time	10^{-6}s	34.58		32.9
Current in transfer line[b]	emA	2.83	3.01	0.108
Current from source[c] (H^+/C^{4+})	emA	4.84	5.14	0.129

Table 4: Beam intensities, results of the present PIMMS review and of the 7 Mev proton variant.

		proton passive spreading, 1st con's set		**Carbon**
Nominal energy	MeV/u	20	7	7
Particles at patient		10^{10}		$4\ 10^{8}$
Particles stored[a]		$3.42\ 10^{10}$		$7.9\ 10^{8}$
Stored current[a]	emA	4.44	2.65	0.368
Particles to inject[b] (H^+/C^{6+})		$3.6\ 10^{10}$		$8.31\ 10^{8}$
Revolution time	10^{-6}s	1.235	2.066	2.058
Injection turns		28	20	16
Effective turns		3.1	2	3.7
Filling time	10^{-6}s	34.58	41.32	32.9
Current in transfer line[b]	emA	1.51	1.38	0.105
Current from source (H^+/C^{4+})	emA	2.58	2.36	0.125

Table 5: Beam intensities, injection in SS-21.

		proton passive spreading, 1st con's set	**Carbon**
Nominal energy	MeV/u	7	7
Particles at patient		10^{10}	$4\ 10^{8}$
Particles stored[a]		$3.4\ 10^{10}$	$7.9\ 10^{8}$
Stored current[a]	emA	2.65	0.368
Particles to inject[b] (H^+/C^{6+})		$3.6\ 10^{10}$	$8.31\ 10^{8}$
Revolution time	10^{-6}s	2.066	2.058
Injection turns		20	16
Effective turns		2.5	2.7
Filling time	10^{-6}s	41.32	32.9
Current in transfer line[b]	emA	1.12	0.143
Current from source (H^+/C^{4+})	emA	1.91	0.171

[a] Next to multiturn injection and scraping

[b] Injected beam, at ring entrance

[c] In [2, PartII,Tab.7.8,p.192], proton intensity, 2nd con's set, is 4.4 emA and Carbon intensity is 0.11 emA, both differing by a coefficient 0.85 from the values listed here as drawn from transmission efficiencies in [2, PartII,Tab.1.6,p.8].

Appendix. Calculation of injection parameters

Simple expressions that give values of injection parameters close to optimum, possibly usable as starting values for finer adjustment, are derived from the geometry of the multiturn injection process.

A Horizontal injection : number of turns

Multiturn injection occurs on near fractional integer tune values of the form $\nu_x \approx 2 - \frac{1}{n}$ ($\nu_x \approx 2 - \frac{1}{3}$ for Carbon, $\nu_x \approx 2 - \frac{1}{4}$ for proton) causing the M injected simulation beamlets to stand on (respectively 3 and 4) spiral arms at the end of the M-turn injection process. Let $n \times \Delta x_{co_{inj}} = a\sigma_x$ be the interval between centers of 2 neighboring beamlets on an arm, with $\Delta x_{co_{inj}} = x_{co_{inj}}/M =$ injection closed orbit bump one-turn step, $\sigma_x = \sqrt{\beta_x \epsilon_{x,inj}/\pi}$ ($\epsilon_{x,inj}$ is the total beamlet surface) and $a =$ some arbitrary value of order $1 - 2$, to be determined (this means that two beamlets overlap a fraction of σ_x).

One can write, $x_{co_{inj}} \approx X_{ESept} + \sigma_x$ ($X_{ESept} =$ position of the injection septum) so that, by substitution of the $\Delta x_{co_{inj}}$ value above,

$$M = \left(1 + \frac{X_{ESept}}{\sqrt{\beta_x \epsilon_{x,inj}/\pi}}\right) \frac{n}{a} \tag{2}$$

The value of the overlapping factor a can be drawn from PIMMS optimization, namely, with $X_{ESept} = 0.041$ m
- for $n = 3$, i.e., in the Carbon case, given $M = 16$ turns, $\beta_x = 8.53$ m, $\epsilon_{x,inj}/\pi = 5\ 10^{-6}$ m.rad, one gets $a \approx 1.30$;
- for $n = 4$, i.e., in the proton injection case, given $M = 28$ turns, $\beta_x = 7.03$ m, $\epsilon_{x,inj}/\pi = 3\ 10^{-6}$ m.rad, one gets $a \approx 1.50$.

7 MeV proton injection The 7 MeV proton injection is realized with $\epsilon_{x,inj}/\pi = 5.1\ 10^{-6}$ m.rad with optical function $\beta_x = 7.03$ m at injection point similar to the 20 MeV injection case and with the same tune so that $n = 4$ entailing $a \approx 1.50$, which yields $M \approx 20$ turns as near optimum injection turn number.

B Vertical injection : Twiss parameters

The injected ellipse is taken rect for simplicity, $\alpha_{z,inj} = 0$; $\beta_{z,inj}$ can be calculated as follows. Known quantities are the vertical emittance to be stored ϵ_z/π, the optical functions at the injection azimuth α_z, β_z, and the injected emittance $\epsilon_{z,inj}/\pi$.

Let us refer to the upper right plot in Fig.13 for illustration ; the injected and stored ellipses intersect on the x axis, so that $\sigma_{inj} + z_{inj} = \sqrt{\epsilon_z/\pi/\gamma_z}$. In addition the opposite end of the injected ellipse is about $\sigma_{inj}/4$ beyond the origin (this is somewhat arbitrary and controls uniformity around the beam axis ; that value has also been retained here

because it fits with PIMMS injection parameters). Hence, $z_{inj} = 3\sigma_{inj}/4$ and $7\sigma_{inj}/4 = 7\sqrt{\beta_{z,inj}\epsilon_{z,inj}/\pi}/4 = \sqrt{\epsilon_z/\pi/\gamma_z}$.
This leads to

$$\beta_{z,inj} = \frac{16}{49}\frac{1}{\gamma_z}\frac{\epsilon_z}{\epsilon_{z,inj}} \tag{3}$$

and to

$$z_{inj} = \frac{3}{4}\sigma_{inj} = \frac{3}{7}\sqrt{\frac{\epsilon_z/\pi}{\gamma_z}} \tag{4}$$

C Geometrical model of the injection process

The coordinates of beamlet #i at turn #N with respect to machine axis in the course of the multiturn process can be calculated as follows.
Let $x_{co,N}$ be the position of the closed orbit at turn #N, in particular $x_{co,0}$ is the initial position, and let x_{inj} be the position of the injected beam. Hence the position of beamlet #i at injection is $\rho_i = x_{inj} - x_{co,N}$.
Let $\bar{x}_i, \bar{x}'_i$ be the coordinates of beamlet #i in the referential centered on x_{co}. One can write $\gamma\bar{x}_i^2 + 2\alpha\bar{x}_i\bar{x}'_i + \beta\bar{x}_i'^2 = \epsilon_i/\pi$. On the other hand, at injection $\begin{cases} \bar{x}_{inj,i} = x_{inj} - x_{co,i} \\ \bar{x}'_{inj,i} = x'_{inj} \end{cases}$, hence ϵ_i/π and the phase $\phi_{0,i}$ of beamlet #i at start.
At the end of turn #N, $\bar{x}_{inj,i} = \sqrt{\beta\epsilon_i/\pi}\cos(2\pi\nu N + \phi_{0,i})$, hence the coordinates $x_{N,i} = x_{co,N} + \bar{x}_{N,i}$ of beamlet #i wrt. the machine axis, whereas $x'_{N,i}$ ensues from the invariant equation above.
It remains to calculate the position $x_{co,N}$ of the closed orbit at turn #N : it is given by $x_{co,N} = x_{co,0} - \frac{N}{M}x_{co}$ with M being the closed orbit bump damping turn number. Eventually the phase advance of beamlet #i at turn #N simply writes $\phi_{N,i} = 2\pi\nu(N-i+1)$. Additional ingredients as the effects on ν, or on $x_{co,N}$, of momentum or amplitude can be included for more precision as illustrated in Fig. 24. The fortran routine follows.

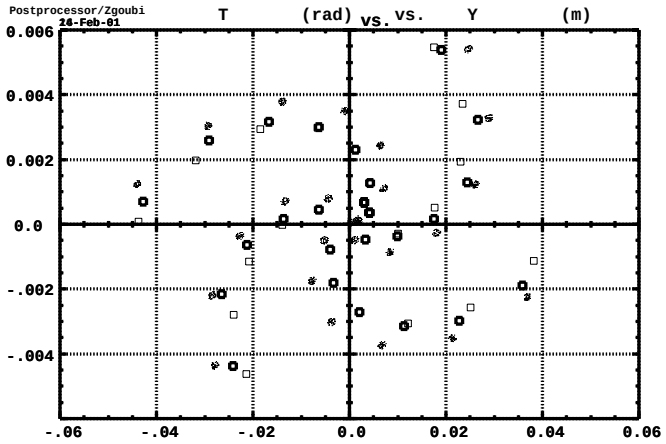

Figure 24: 7 MeV proton injection into SS-21, 28 turns injected, H phase space observed at injection septum at end of turn 28. Squares=analytical model, including (closest squares to the beamlets) or exclusive of (furthest squares) momentum and amplitude detuning effects.

```
C Multiturn injection, simulation routine.

      dimension xbarinj(28), xco(28), xpbarinj(28), epspi(28), phi0(28)
      dimension xbar(30,28),xpbar(30,28), x(30,28), xp(30,28)
      pi = 4.*atan(1.)
      xnu0=1.68000044
      dpp = -.0021
      xsi = -3.58
      dnudE = 37.5
      ntour=16
      ipaq=16
      xinj=-0.0476
      xpinj=0.
      xco0 = -0.04406   ! pour dpp=0,  ou  -4.3923E-02 pour dpp=-0.0021
      beta = 8.527749
      alpha = -.162483
      gamma = (1.+alpha*alpha)/beta
C paquet # i
      do i = 1, ipaq
        xco(i) = (1.d0 - float(i-1)/float(ntour)) * xco0
        xbarinj(i) = xinj - xco(i)
        xpbarinj(i) = xpinj
        epspi(i) = gamma*xbarinj(i)**2 + 2. * alpha * xbarinj(i)*
     >     xpbarinj(i) + beta *xpbarinj(i)**2
        phi0(i) = atan2(xpbarinj(i) ,xbarinj(i) )
C a la fin du tour # n
        qtour = 0
        do n=i,ntour
          qtour = qtour + 1
          xnu = xnu0
          iter = 0
 20       continue
          dphi = 2.*pi*xnu*qtour
          xbar(n,i) = sqrt(beta*epspi(i)) *
     >              cos (dphi + phi0(i))
          xpbar(n,i)=-(sqrt(beta*epspi(i)) *sin(dphi +
     >        phi0(i)) + alpha * xbar(n,i) ) / beta
          x(n,i) = xco(i) - qtour* xco0/float(ntour) + xbar(n,i)
          xp(n,i) = xpbar(n,i)
C------- Detuning d'ampliude
          dnuC0 = dnudE * x(n,i)*x(n,i)/beta
          xnu = xnu0 + dnuC0
          if (iter.lt.2) then
            iter=iter+1
            goto 20
          endif
          write(6,*) n,x(n,i)
c          if(i.eq.10) write(88,*) x(n,i) ,xp(n,i)
        enddo
        n = ntour
        write(88,fmt='(1p,2e14.6,i4)') x(n,i),xp(n,i),i
      enddo
      stop
      end
```

References

[1] Projet d'un centre d'hadronthérapie par faisceaux d'ions carbone, Mise à jour janvier 2001, M. Bajard, J. P. Gérard, J. Remillieux, D. Sappey-Marinier, UCB-Lyon 1.

[2] Proton-ion medical machine study, Part I, CERN/PS 99-010 (DI) March 1999 & Part II, CERN/PS 2000-007 (DR) May 2000.

[3] BETA optics code, J. Payet et als., CEA DSM/DAPNIA/SEA, Saclay.

[4] Zgoubi users' guide, F. Méot and S. Valéro, report CEA-Saclay DSM/DAPNIA/SEA-97-13 (Oct. 1997) ; The ray-tracing code Zgoubi, F. Méot, NIM A 427 (1999) 353-356.

[5] AGILE program for synchrotron lattice design, P. J. Bryant, http://nicewww.cern.ch/-bryant.

[6] MAD user's guide, H. Grote, C. Iselin, http://mad.home.cern.ch/mad/

[7] Projet d'hadronthérapie Rhône-Alpes, Cahier des charges de l'injecteur, to be published.

[8] Technical group meeting minutes, HT-1 06/11/2000, HT-2 01/2001 & HT-3 28/01/2000, F. Méot, DSM/DAPNIA/SEA, CEA Saclay.